Thesis Formulation Report

University of Bath

Katie Phillips

Elucidating the lubrication layer for impacting droplets

Abstract

In this report we investigate the air layer between a body of fluid and a Faraday forced bouncing droplet. We elucidate the lubrication air layer dynamics and provide information on the pressure transmission between the droplet and the main fluid body. The lubrication layer model will then consider its two different boundaries: the boundaries where the air and fluid interact, and the boundary where the lubrication layer dissipates which acts as an inlet/outlet to the rest of the air.

Contents

Acknowledgements

I'd like to thank Professor Paul Milewski and Professor Jonathan Evans for guiding me throughout this project with their excellent supervision and continued motivation, and EPSRC for their financial support. I'd also like to thank SAMBa and especially Dr Susie Douglas for ensuring that I had a supportive and welcoming environment to work in. I wouldn't have been able to write this report (almost literally) without the support of my wonderful partner Allen, who enabled me to concentrate on my work and ensured we always had internet whilst we moved house. Finally I'd like to thank my fellow Cohort 6 SAMBa students, without whom I'm sure I wouldn't have enjoyed this process half as much.

Responsible Research and Innovation

This project concerns researching theoretical aspects of a fluid mechanics problem. The physical system that this project is concerned with occurs rarely in nature or in industrial applications, though the excited Faraday waves can be found incidentally in aligator mating displays or in shamanic use of tibetan singing bowls. As such the research undertaken in this project is still within the the early stages of the fields timeline. This fundamental research is still purely theoretical but on a long timescale could have unknown benefits. Industrially, Faraday generated droplets are used in medical equipment such as nebulisers, which are drug delivery machines used predominantely by people with lung conditions to inhale medicine. Though there aren't any direct links between the research in this paper and industry so far, there is still great potential with future research. As such there is little ethical issue to be considered when working in this area, however, I have, to the best of my ability undertaken this project whilst keeping aware of any potential applications of the research or upcoming uses in the field. Fluid dynamics as a larger field has many applications in transport, aerodynamics, and instustrial applications so I remain aware of the potential implications any development may have.

1 Introduction

When a droplet lands on a bath of the same fluid, it usually coalesces with the bath due to the Van der Waal forces between the fluids. However, in certain parameter regimes a lubrication air layer forms and delays coalescence by separating the drop and bath so that the capillary forces on the surface of the bath have time to propel the droplet upwards before the air layer is depleated. As such the droplet is propelled upwards and bounces off the surface. In addition, if the bath is vibrating vertically, then the droplet can be bounced periodically, indefinitely delaying coalescence. This introduces a variety of complex phenomena, dependant on the physical parameters of the system, such as droplets bouncing in place [5], or being propelled laterally in a walking state [10], as depicted in Figure 1.

It is the aim of this report, and the continuing work beyond it, to improve the understanding and model the as yet poorly understood lubrication air layer. This will allow for a full understanding of the phenomena. Most studies on the problem so far neglect to include the air layer as a component, instead using different methods to consider the pressure transfer. For example a point-forcing term to replace the droplet [7], or replacing the air layer with a kinematic matching condition [12] between the droplet and bath. Until recently numerical or experimental results for this lubrication air layer were not available. Full Navier Stokes numerical studies [11, 3] are now possible but are far too computationally intensive to be a feasible approach for this phenomena. By considering the problem with lubrication theory we aim to produce a more viable method of including the air layer to the system.

We first present a review on the current literature for the study of pilot-wave dynamics. In Chapter 2 we focus on the development of a numerical scheme to model the evolution of the surface of a Faraday forced bath when subject to a vertical pressure forcing, by following the work done in a paper by Milewski et al [15]. Chapter 3 then steps away from the global picture of bouncing droplets and focuses locally on deriving the lubrication equations for a system consisting of a vertical layering of a thin air lubrication layer between a fluid bath and a sphere moving with arbitrary velocity.

Figure 1: Photo of a walking droplet [18]

1.1 Literature review

Prior to the inclusion of a droplet to the system, Benjamin and Ursell [1] discovered that above an amplitudal threshold (Γ_F), standing Faraday waves could form on the surface of a vibrating bath. This was further developed by Kumar and Tuckerman [14] who considered the stability of the waves under different fluid properites, emphasisng the role of viscosity to the system. Walker [20] showed that a droplet could 'float' on a vertically vibrating bath but it was in 2005 that Couder et al [5] first discovered that droplets could bounce periodically on a vibrating bath.

Eddi et al [10] showed that as the acceleration amplitude approaches the Faraday threshhold from below, these bouncing droplets can walk along the surface of the bath. This is due to a lateral 'kick' coming from the drop landing on an uneven surface, interacting with their previously generated wave field. Thus recreating a pilot-wave system that was first hypothesised by De Broglie [6] as an explanation for quantum behaviour. This hydrodynamic pilot-wave system initially found by Couder acts as a macroscopic analogy for many quantum phenomena. This analgous behaviour has ben reexamined by Bush through a series of experiments [2].

Submerged topography, by this we mean the introduction of complex geometries such as walls beneath the surface of the fluid, can have an affect the droplets motion and can be used to replicate results in quantum phenomena on a macroscopic scale. Couder and Fort [4] modelled the trajectory of a droplet over a submerged single and double slit and demonstrated a statistical behaviour similar to that of a single quantum particle passing through the analagous geometry with similar diffraction. Similarly, Eddi et al [9] used submerged walls to show similar behaviour to that of quantum tunnelling. A droplet will tunnel across a sumberged wall with increasing probability as the width of the wall decreases. Harris et al [13] showed that a walker in a circular bath has a similar probability density function to that of an electron in a quantum corral.

There has been a decent amount of work done on pilot-wave hydrodynamics that eliminate the droplet all together. Durey et al [7] don't consider the droplet as much as wave generation through point-forcing. This allowed the solution of the waves to be written semi-analytically through the use of greens functions [8]. In constrast, Galeano [12] does have a body falling onto a bath, but now consider a solid hydrophobic sphere as a replacement for a droplet. The hydrophobic nature of the sphere allows for the assumption that the free surface is tangential to the sphere's surface, and allows for the disregard of droplet deformation. We utilise these methods of simplifying the system in chapters 2 and 3 respectively, with the intention of developing work that can replace mehtods.

2 Faraday Waves

In this chapter we introduce the standard notation used when considering Faraday waves, and discuss the requirements of different pilot-wave modes. We then follow the work done in the 2015 paper by Milewski et al's [15], and develop our own numerical simulations based upon this work. Finally we discuss the numerical results obtained.

When vibrated, the bath is subject to a sinusoidal vibration with angular frequency ω_0 and amplitute A. The stability of the system is then governed by the acceleration amplitude $\Gamma = A\omega_0^2$. Above a certain threshold $\Gamma = \Gamma_F$ the surface of the bath becomes independently unstable and forms standing Faraday waves, as such, this threshold is called the Faraday frequency.

Below this threshold there are different regimes:

- $\Gamma < \Gamma_B$: The vibrational frequency is too low to sustain bouncing and the droplet and bath coalesce.
- $\Gamma_B < \Gamma < \Gamma_W$: The droplet bounces on the surface of the fluid, either in a periodic or chaotic motion.
- $\Gamma_W < \Gamma < \Gamma_C$: The droplet interacts with its wave field and has a horizontal motion - it begins to 'walk' along the surface of the fluid.
- $\Gamma_C < \Gamma < \Gamma_F$: Chaotic motion arises as the memory time of previous impacts affects the droplets motion.
- $\Gamma_F < \Gamma$: The free surface becomes unstable and develops Faraday waves without the droplet. Pilot-wave dynamics are no longer in effect.

The Faraday threshold Γ_F of a fluid is dependent on physical factors such as viscosity/density of the fluid or the shape of the bath. Furthermore the subcritical thresholds Γ_B or Γ_W also depend on these factors, as well as the droplet size, as was determined by Protiere et al [19].

In the subcritical regime $\Gamma_B < \Gamma < \Gamma_F$, the droplets motion produces axisymmetric standing Faraday waves eminating out from the center of the droplets bounce. This relationship between the droplets and the wave-field it creates is called the pilot-wave.

A bouncing droplet has a state dictated by n bounces in m forcing periods and has a mode ordering p, the state is denoted by $(m, n)^p$. The largest p is the most energetic mode. For example if a droplet bounces once every two forcing periods, the state would be $(2, 1)^p$ with different p for the different modes.

In the rest of this chapter we follow the calculations by Milewski et al [15], where they derive an equation that couples the droplets bouncing motion with an evolution of the wave-field generated. We will use their computation to develop a numerical code that will model simplified model of a vibrating bath subject to a periodic pressure forcing term from above. They model the vertical dynamics as a non-linear spring, first done by Moláček and Bush [17]. However we intend to replace this method with our own evolution of the pressure later on (see Chapter 3) so instead will use a self-generated term for the pressure, motivated by the physical system and previous experimental and numerical results. We consider the pressure from the droplet to be given by $\mathbf{P}_D(x, y, t)$ where there is a combination of a 'bouncing frequency' and a function describing the shape of the pressure acting on the surface.

2.1 Linear quasi-potential model

In this section we summarise the linear quasi-potential model of [15], which provides a simple framework for the generalisation to transient Faraday waves due to a given time varying peridoic pressure forcing.

Considering the vertical as the z direction and letting the xy-plane be the horizontal, we consider an incompresssible viscous fluid in an infinite depth.

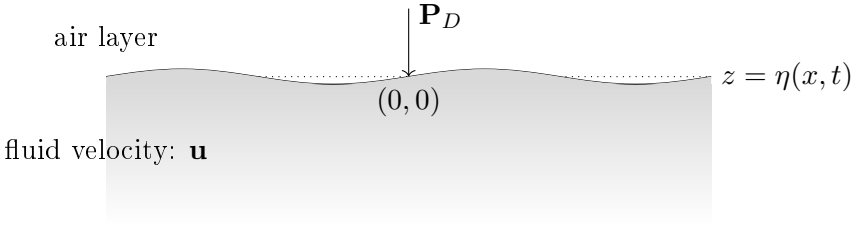

Figure 2: Bath domain with arbitrary pressure from droplet.

The fluid in the bath is goverened by the full Navier-Stokes equations. At the air-fluid interface, given by $z = \eta(x,y,t)$, there are two boundary conditions: the kinematic boundary condition (KBC) and the dynamic pressure-matching condition (DBC). The KBC is given by $\frac{D}{Dt}(\eta - x) = 0$ and means that the free surface moves with the velocity of the fluid at the surface. The DBC dictates that pressure must be continuous across the interface. The DBC contains the external pressure forcing term that comes from the droplet. Furthermore,there is an expected decay of velocity away from the interface. For the velocity field $\mathbf{u} = \mathbf{u}(x,y,z,t)$ of the fluid, with pressure $p = p(x,y,z,t)$, and constant kinematic viscosity ν and surface tension σ, the governing system of equations are listed below.

$$\mathbf{u}_t + \mathbf{u}\cdot\nabla\mathbf{u} = -\nabla p + \nu\nabla^2\mathbf{u} + \mathbf{F}(t) \qquad z \le \eta(x,y,t) \tag{2.1}$$

$$\nabla\cdot\mathbf{u} = 0 \qquad z \le \eta(x,y,t) \tag{2.2}$$

$$\mathbf{u} \to 0 \qquad z \to -\infty \tag{2.3}$$

$$\eta_t + \mathbf{u}\cdot\nabla(\eta - z) = 0 \qquad z = \eta(x,y,t) \tag{2.4}$$

$$p\mathbf{n} - \boldsymbol{\tau}\cdot\mathbf{n} = \sigma\kappa\mathbf{n} + \mathbf{P}_D(x,y,t)\mathbf{n} \qquad z = \eta(x,y,t) \tag{2.5}$$

Where $\mathbf{F}(t) = -(g + g\Gamma\cos(\omega_0 t))\mathbf{z}$ includes the vibrational forcing energy and gravity acting downwards. In the above equations, $\boldsymbol{\tau}$ is the strain tensor given by $(\nabla\mathbf{u} + \nabla\mathbf{u}^\top)$, $\kappa = \nabla\cdot\mathbf{n}$ is the curvature of the free surface, and $\mathbf{P}_D$ is the pressure coming from the droplet.

Following the work done by Milewski et al (2015) [15], we assume that the wave slope is shallow and waves have small amplitute so we can consider the linearised system. Assuming to leading order the flow is irrotational and inviscid we use the Helmholtz substitution $\mathbf{u} = \nabla\phi + \varepsilon\nabla\times\boldsymbol{\Psi}$ for a scalar potential ϕ and rotational vector potential $\boldsymbol{\Psi}$. This results in the system

$$\Delta\phi = 0 \qquad z \le 0 \tag{2.6}$$

$$\phi \to 0 \qquad z \to \infty \tag{2.7}$$

$$\phi_t = -g(t)\eta + \frac{\sigma}{\rho}\Delta_H\eta + 2\nu\Delta_H\phi - \frac{1}{\rho}\mathbf{P}_D \qquad z = 0 \tag{2.8}$$

$$\eta_t = \phi_z + 2\nu\Delta_H\eta \qquad z = 0 \tag{2.9}$$

for $g(t) = g(1 - \Gamma\cos(\omega_0 t))$ and Δ_H is the horizontal laplacian $\partial^2/\partial x^2 + \partial^2/\partial y^2$

2.1.1 Generating a pressure forcing term

We consider the pressure from the droplet, $\mathbf{P}_D$ as a forcing term over a specific area. In [15] it was written succintly as

$$\mathbf{P}_D = \frac{F(t)}{\pi R(t)^2},$$

where $F(t)$ is a function of the force, and $R(t)$ is the effective radius so that $\pi R(t)^2$ is the contact area of the bath and droplet - meaning the thickness of the air layer within this area is sufficiently small enough to mimick contact. This is illustrated in Figure 3. Following the assumption that the slope of the free surface is small, the relative contact radius must be smaller than the radius of the droplet R_0 (ignoring deformation). If the bath were to have $R(t) = R_0$ then the free surface tangential to the droplet at that point would have slope significantly greater than 1, which is contadictory. Following the results in Galeano's paper [12] we can say that $R(t)/R_0 \approx \sqrt{0.2}$, so an assumption that $R(t)$ is approximately half of R_0 is reasonable.

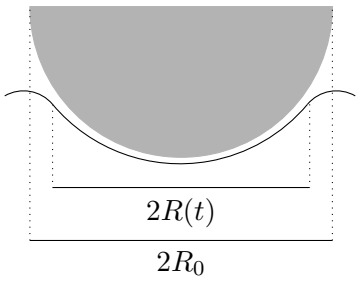

Figure 3: Illustration of the difference between the radius of the droplet R_0 and the radius of the lubrication layer, sometimes called the 'effective' radius $R(t)$

When we discuss the modes of the system, there are different periods that couple together. For an (m, n) mode there are n bounces in m forcing periods. We let T_F denote the forcing period which is perscribed in experiments (In our case is $T_F = \omega_0/2\pi$). Amplitudes above the Faraday threshold, Γ_F, excite standing Faraday waves on the free surface without any requirement for pressure forcing, and these waves are subharmonic with period $T_{Faraday} = 2T_F$. Further on we use the notation T_P to describe the period of our pressure forcing, however it is worth noting that this period cannot be predetermined when including a real droplet.

For a system that includes droplet dynamics, the (m, n) mode is ascertained from the results of the simulation, depending on the parameters and conditions of the system. However, for a pretedermined pressure-forcing, we perscribe the period and thus the mode. As such we choose to model the $(2, 1)$ mode as it is one of the more stable bouncing modes. The $(2, 1)$ mode is such that for every two vibration periods the droplet bounces once. This means the droplet's period synchronises with the Faraday waves in a complicated non-linear way. The $(2, 1)$ mode arises at frequencies closer to the Faraday threshhold, than say the $(1, 1)$ mode which has a single bounce every forcing period.

By looking at numerical results from Galeano's paper [12], they simulate the force between the bath and the droplet (or in their case hydrophobic sphere), as an instantaneous impact of the droplet which then decays linearly back to zero until the point of liftoff. This is sketched out in Figure 4.

This force function is constrained by its impulse being periodic, i.e. for m the mass of the droplet and g acceleration due to gravity, the integral over any one period is constant

$$\int_0^T F(t)dt = mgT_p,$$

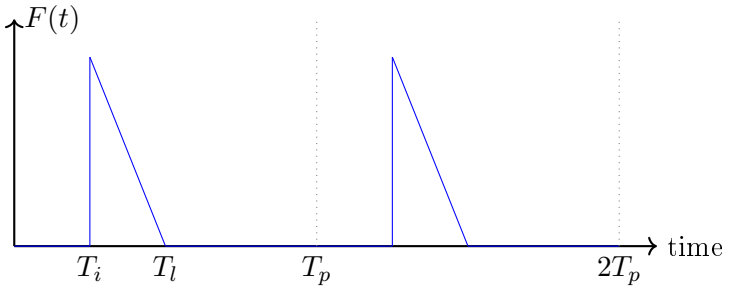

Figure 4: Sketch of force $F(t)$ acting from the droplet.

for T_i the time of impulse, T_l the time of liftoff, and T_p the pressure forcing period as described above. The equation of force we used in the code is then given by

$$F(t) = \frac{2mgT_p}{(T_l - T_i)^2}(T_l - t), \qquad \text{mod } T_p.$$

2.2 The spectral method

To obtain numerical results for this system we follow the spectral method. Introduce the notation $\mathcal{F}$ to be the Fourier transform and $\mathcal{F}^{-1}$ to be its inverse, as such we denote $\mathcal{F}[\phi]$ with $\hat{\phi}$. We are then able to make the transformations:

$$\phi_z = \mathcal{F}^{-1}[k\hat{\phi}]$$
$$\Delta_H \phi = \mathcal{F}^{-1}[-(k_x^2 + k_y^2)\hat{\phi}]$$

for $k = \sqrt{k_x^2 + k_y^2}$ and similar for the horizontal laplacian of η. This gives the Fourier mode of the boundary equations (2.6)-(2.9) to be

$$\hat{\phi}_t = -g(t)\hat{\eta} - \frac{\sigma}{\rho}(k_x^2 + k_y^2)\hat{\eta} - 2\nu(k_x^2 + k_y^2)\hat{\phi} - \frac{1}{\rho}\hat{P}_D(t), \tag{2.10}$$
$$\hat{\eta}_t = k\hat{\phi} - 2\nu(k_x^2 + k_y^2)\hat{\eta}, \tag{2.11}$$

where $\hat{P}_D$ is the Fourier transform of the pressure arising from the droplet. This coupled system of equations can be solved numerically.

2.3 Description of numerical results

We used the dimensional equations in the code, and solved over a quare domain of side length 0.1 m^2, though the true solution is unbounded in the horizontal. We used parameter values from Table 1, and used 512×512 Fourier modes in space. The code ran in Matlab using the built in `fft2` function to take fast Fourier transforms and `ifft2` for their inverse transforms. Due to the stiffness of the diffusive laplacian Δ_H, a time step of $h = 1 \times 10^{-5}$ was used to ensure the stability of the code. All results are plotted with spatial values in m and time in m For all of the results we maintain a $(2, 1)$ mode and, unless specified, default to $\Gamma = 3$, with a Faraday threshold at $\Gamma_F = 4.22$.

Figure 5 plots the evolution of a single point in the free surface over time. The point specified is at the centre of the grid directly beneath the pressure forcing. It demonstrates clearly the periodic surface displacement which occurs at any signle point. The sharp spike downwards on the graph coincides with the impact of the pressure forcing term at time $T_i = 0.5T_F$ (625 timesteps). Liftoff of the droplet from the bath occurs at $T_l = T_F$ (1250 timesteps). The period

Parameter	Symbol	Value
surface tension	σ	20.6×10^{-3} kg s^{-2}
fluid density	ρ	949 kg m^{-3}
kinematic viscosity	$\nu = \mu/\rho$	2×10^{-5}m^2 s^{-1}
dynamic viscosity (air)	μ^a	1.8×10^{-5}kg m^{-1} s^{-1}
acceleration due to gravity	g	9.8 m s^{-2}
angular frequency	ω_0	$80 \times 2\pi$ s^{-1}
radius of droplet	R_0	3.8×10^{-4} m

Table 1: Values of physical parameters used in code for the given systems

T_p of the pressure forcing is then $2T_F$ (2500 timesteps). As Γ is sufficiently small in comparison to the Faraday threshhold, Γ_F, the stystem reaches a steady state period quickly. This is expected as the system is analagous to a simple forced-damped system, as the pressure term adds energy to the wave and the viscosity of the fluid dampens the effect, so a steady state periodic system is expected.

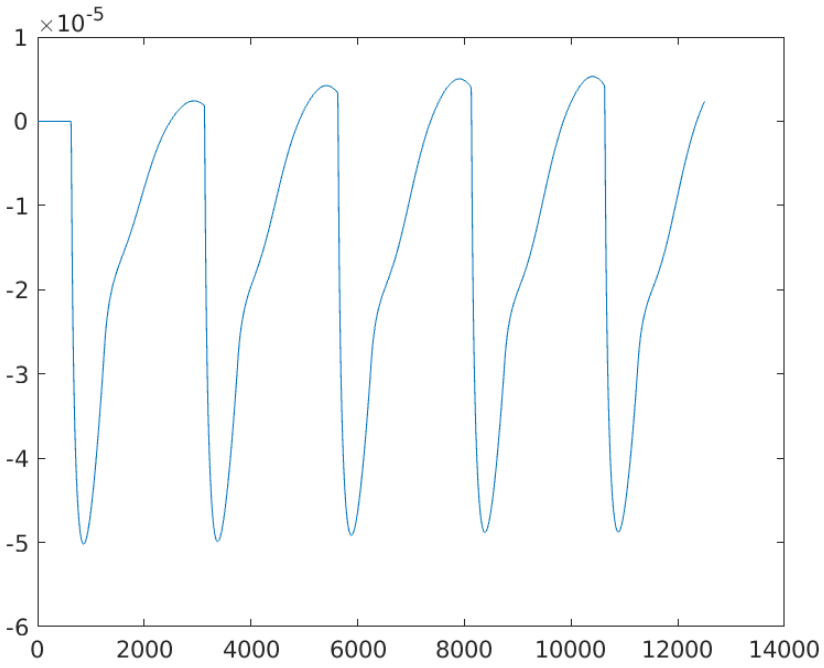

Figure 5: Tracking the point of the fluid bath beneath the centre of the droplets presure forcing. Vertical axis is displacement (m), and horizontal axis tracks evolution in time (*timesteps*). Evolution over total Time $T = 10T_F$, and run with parameters from Table 1 and $\Gamma = 3$.

Since the problem is axisymmetric, any wave profile passing through the origin will be identical, thus Figure 6 gives the full wave-field of the solution. This can be imagined as rotating the wave profile around the vertical axis to give the full solution. The progression (a)-(i) depicts the full steady state cycle. As Figures (a)-(i) are a full period, Figure (j) further illustrates the periodicity of the solution as it is the same as Figure (a). It is clear to see the system is dominated by the narrow pressure forcing occuring at 0 on the horizontal axis. The presure forcing occurs at $0.5T_F \pmod{T_P}$ so for this period occurs just before Figure (d), and lasts until Figure (f). These figures act to emphasise the oddity of the multiscale problem that arise due to the Faraday resonance. For a narrow pressure forcing of radius $\mathcal{O}(10^{-4}\text{m})$, significantly longer wavelengths of $\mathcal{O}(0.1\text{m})$ are produced.

In Figure 7, each row consists of a simulation run over 20 forcing periods, with the figures taken at $2T_F$, $8T_F$ and $20T_F$. Each row corresponds to a different value of Γ, varying from no forcing amplitude $\Gamma = 0$ up to the Faraday threshold, $\Gamma_F = 4.22$. These images depict the effect of increasing the forcing amplitude on the surface waves produced. At $\Gamma = 0$ there is no Faraday wave formation, however as Γ is increased it induces a quasi-standing wave on the macroscopic scale that becomes more and more pronounced. However as Γ approaches the Faraday threshold, Γ_F, the system takes longer to reach its periodic steady state. These images are coupled with Figure 8, as it is a superposition of an axial cross-section (any line across the domain passing through the origin - all identical due to the axisymmetry of the problem) of the figures (e,f,i,l,o) in Figure 7. Figure 8 shows that increasing the forcing amplitude increases the amplitude of the resulting Faraday waves. Furthermore, Figure 8 depicts larger forcing amplitudes having a longer decay as their resulting Faraday waves reach further out from the origin.

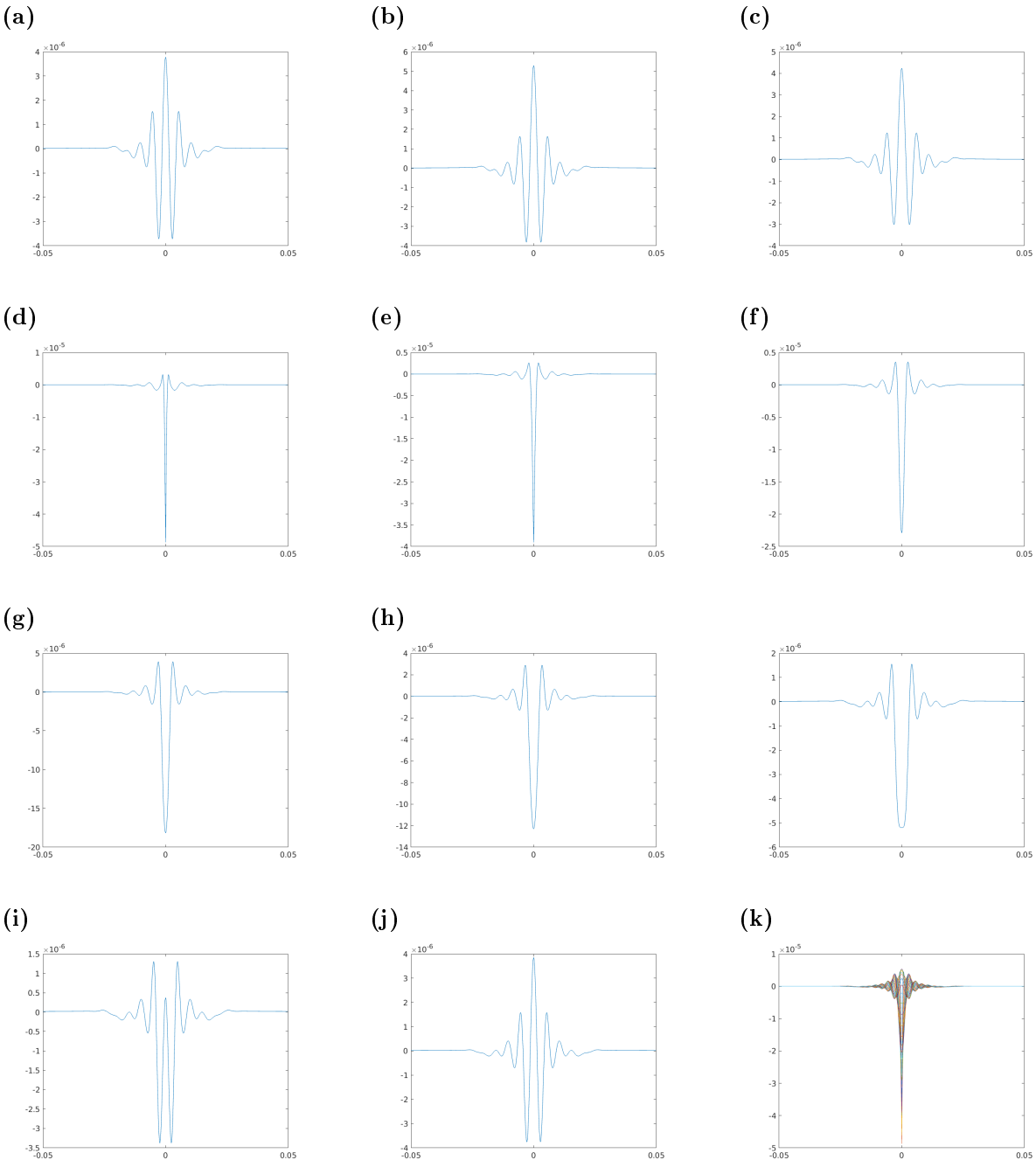

Figure 6: The cross section of the (axisymmetric) wave profile evolution for one complete $(2,1)$ period T_P from $T = 8T_F$ to $T = 10T_F$ ran at $\Gamma = 3$. Both axes have units of length, given in m. Subfigures (a)-(j) are a progression in time (with a difference of 250 timesteps$/0.0025s$ between graph), acompanied by an superposition of the entire period T_P.

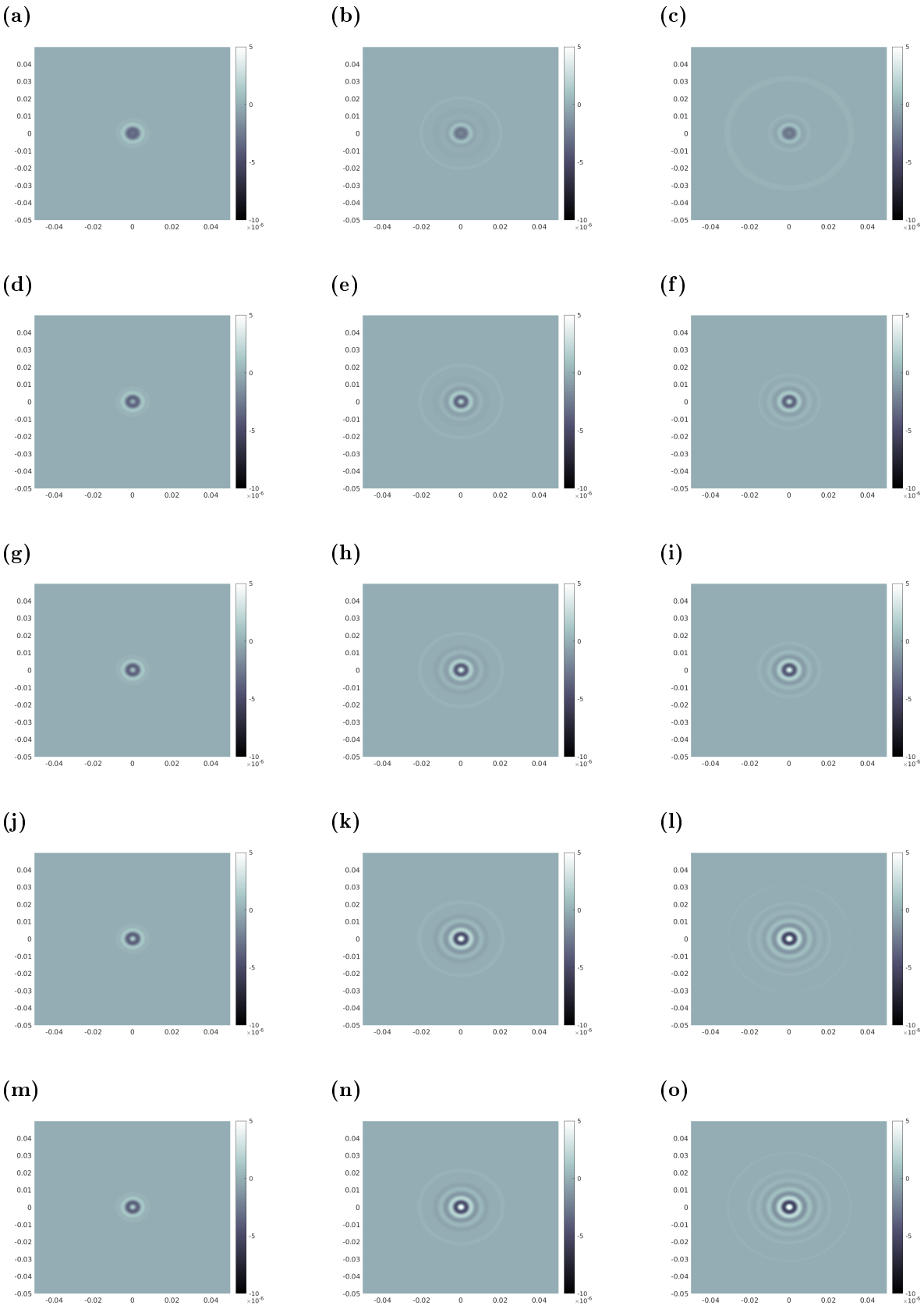

Figure 7: Aerial view of solution domain taken over different time steps with different forcing amplitudes Γ with continued periodic forcing from the pressure term $\mathbf{P}_D$ defined previously. Times are at $T = 2T_F$ (a,d,g,j,m), $T = 8T_F$ (b,e,h,k,n) and $T + 20T_F$ (c,f,i,l,o). $\Gamma = 0$ (a-c), $\Gamma = 3$ (d-f), $\Gamma = 3.6$ (g-i), $\Gamma = 4.15$ (j-l) ,$\Gamma = 4.22$ (m-o). Colour gradient indicates vertical displacement, in m.

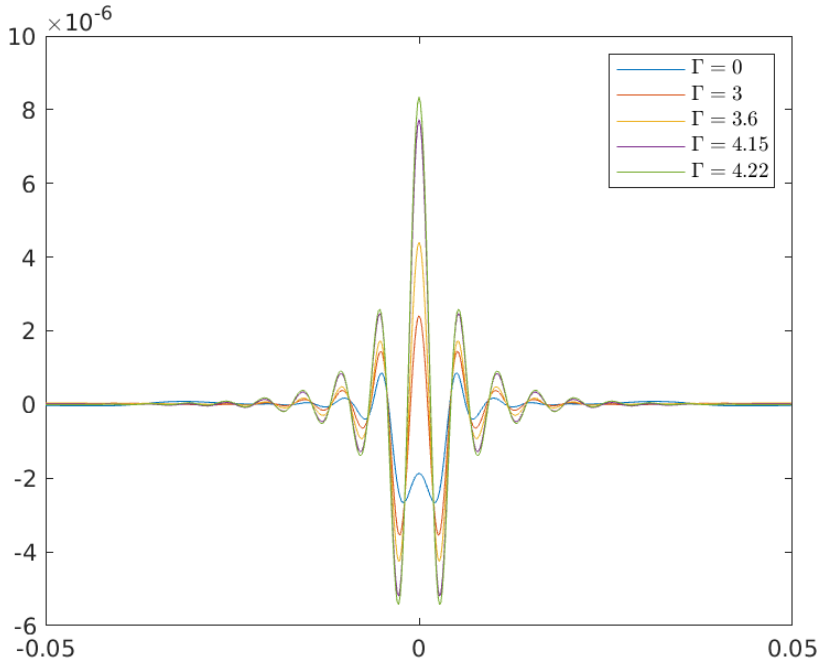

Figure 8: Superposition of axial (m) cross-section of Figure 7 (e,f,i,l,o). i.e changing Γ but all taken at time $T = 20T_F$. Visible increase in amplitude of resulting Faraday waves with increase in Γ. Axis are in m and each line represents a simulation run with distinct Γ.

3 Lubrication Theory

3.1 Motivation

During the flight of a bouncing droplet on a bath, there is a 'contact' made between the two where a thin air layer acts as a transfer for the pressure between droplet and bath, preventing coalescence of the two bodies of fluid. Within a certain radius of the droplet ($R(t)$) this air layer is understood to have a constant thickness $h(t)$ that is significantly smaller than the effective radius. Refer back to Chapter 2 for a more in depth explanation.

Lubrication theory is used when one dimension is significantly smaller than the others, usually named the height or thickness of the geometry. This discrepancy between the lengthscales means the fluid layer can take a relatively large normal load whilst providing little resistance to the tangential motion, thus acting as a lubricant between the two bodies. If we consider the fluid droplet and bath as the two bodies in question, then the geometry of the air layer satisfies the requirements for lubrication theory to be applied.

In this chapter we use lubrication theory to develop a system of equations that govern the pressure transfer happening within this air layer. The work in this chapter is motivated by the paper by Galeano [12], in which the pilot-wave dynamics are considered using a kinematic-matching condition to model the pressure transfer from the droplet to the bath. It considers a rigid hydrophobic sphere that is in partial contact with the surface of the bath at a constant contact angle (180°). The lubrication theory work considered within this chapter will replace this kinematic matching condition.

The phenomena of air sandwiched between two bodies of fluid, both with the same density, is highly unlikely to occur in practice.Up until the discovery of the Faraday bouncers, excluding a few parameter regimes, droplets would coalesce with the bath as the air layer shrinks due to the Van-der-Waals forces between the droplet and the bath. The literature on multilayered flows, therefore, tends to considered fluids with increasing density as that is the most stable state. As such we begin the development of the lubrication layer theory in the simplest case. Modeling the droplet as a hydrophobic sphere so that we may ignore surface tension and pressure matching at the boundary of the sphere, means we don't have to consider the effect of deformation of the droplet. We also consider a non-vibrating system for simplicity, but derive the system in such a way that future inclusion has been considered. We do include arbitrary velocity for the sphere, rather than unidirectional falling, so we may include walking droplets in the future.

3.2 Lubrication layer for a hydrophobic sphere

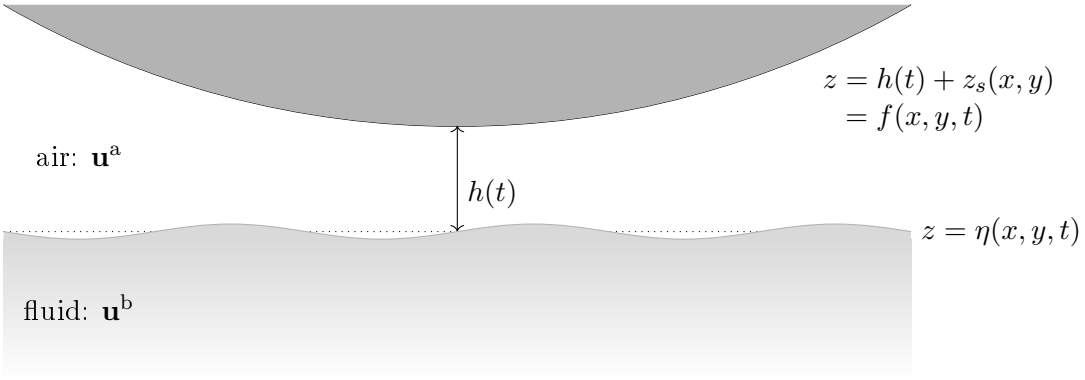

Figure 9: Hydrophobic Sphere with geometry $z_s(x, y, t)$ a distance $h(t)$ above a liquid bath that has free surface $z = \eta(x, y, t)$ which if at rest lies along $z = 0$. Between them is a lubrication air layer.

We consider a 3D system, depicted in Figure 9 with the solid sphere at the top with a rigid and impermeable surface. The air layer then lies beneath the sphere and above a fluid bath, with an interfacial wave between the lower two. We consider cartesian coordinates (x, y, z) with positive z being upwards. For the purposes of this chapter only we model the air layer as having constant thickness $h(t)$ and for the consideration of lubrication theory only consider the time when this thickness is significantly smaller than the radius of the air layer $R(t)$ (with $R(t) \leq R_0$). The surface of the sphere is given by the height of the air layer plus the geometry of the sphere, i.e $z = h(t) + z_s(x, y)$ and will be denoted by the function $z = f(x, y, t)$, the equation perscribing the interface between the fluid bath and the air layer given by $z = \eta(x, y, t)$

The air and bath fluid regimes will be described with superscripts $\cdot^a$ and $\cdot^b$ respectively. For example the two fluids have velocities given by $\mathbf{u}^{\mathrm{a}} = (\mathrm{u}^{\mathrm{a}}, \mathrm{v}^{\mathrm{a}}, \mathrm{w}^{\mathrm{a}})$ and $\mathbf{u}^{\mathrm{b}} = (\mathrm{u}^{\mathrm{b}}, \mathrm{v}^{\mathrm{b}}, \mathrm{w}^{\mathrm{b}})$. Both fluids are modelled with full Navier-Stokes equations. On the interface between the air and bath given by $z = \eta(x, y, t)$, there is the kinematic boundary condition $\frac{D}{Dt}(\eta - z) = 0$, and a pressure matching condition along each axis. At the surface of the sphere there are no-slip and no-penetration conditions, ensuring that the air velocity $\mathbf{u}^{\mathrm{a}}$ matches the velocity of the sphere $\mathbf{U}_{\mathrm{sphere}}$, and there is no flow in or out of the sphere, respectively. Let

- $\mu^{\cdot}$ denote the constant dynamic viscosity $_{(\cdot=a,b)}$,
- $\sigma^{\cdot}$ denote the stress tensor $_{(\cdot=a,b)}$,
- $\rho^{\cdot}$ denote the constant density $_{(\cdot=a,b)}$,
- $p^{\cdot} = p^{\cdot}(x, y, z, t)$ denote the pressure $_{(\cdot=a,b)}$,
- $\mathbf{n}$ denote the outward unit normal of the free surface,
- $\mathbf{m}_x$, $\mathbf{m}_y$ denote the two unit tangents of the free surface,
- $\mathbf{g} = -g\mathbf{z}$ denote gravitational acceleration.

The full system of governing equations are then listed below in descending height order.

$$\mathbf{u}^{\mathrm{a}} = \mathbf{U}_{\text{sphere}} \qquad z = f(x,y,t) \tag{3.1}$$

$$\mathbf{u}^{\mathrm{a}} \cdot \mathbf{n} = \mathbf{U}_{\text{sphere}} \cdot \mathbf{n} \qquad z = f(x,y,t) \tag{3.2}$$

$$\rho^{\mathrm{a}}(\mathbf{u}^{\mathrm{a}}{}_t + (\mathbf{u}^{\mathrm{a}} \cdot \nabla)\,\mathbf{u}^{\mathrm{a}}) = -\nabla\,\mathrm{p}^{\mathrm{a}} + \mu^{\mathrm{a}}\,\nabla^2\,\mathbf{u}^{\mathrm{a}} - \mathbf{g}\,\rho^{\mathrm{a}} \qquad \eta(x,y,t) < z < f(x,y,t) \tag{3.3}$$

$$\nabla \cdot \mathbf{u}^{\mathrm{a}} = 0 \qquad \eta(x,y,t) < z < f(x,y,t) \tag{3.4}$$

$$\eta_t + \mathrm{u}^{\mathrm{a}}\,\eta_x + \mathrm{v}^{\mathrm{a}}\,\eta_y = \mathrm{w}^{\mathrm{a}} \qquad z = \eta(x,y,t) \tag{3.5}$$

$$\mathbf{n} \cdot \sigma^{\mathrm{b}} \cdot \mathbf{n} - \mathbf{n} \cdot \sigma^{\mathrm{a}} \cdot \mathbf{n} = \sigma(\nabla \cdot \mathbf{n}) \qquad z = \eta(x,y,t) \tag{3.6}$$

$$\mathbf{m}_x \cdot \sigma^{\mathrm{b}} \cdot \mathbf{n} - \mathbf{m}_x \cdot \sigma^{\mathrm{a}} \cdot \mathbf{n} = 0 \qquad z = \eta(x,y,t) \tag{3.7}$$

$$\mathbf{m}_y \cdot \sigma^{\mathrm{b}} \cdot \mathbf{n} - \mathbf{m}_y \cdot \sigma^{\mathrm{a}} \cdot \mathbf{n} = 0 \qquad z = \eta(x,y,t) \tag{3.8}$$

$$\rho^{\mathrm{b}}(\mathbf{u}^{\mathrm{b}}{}_t + (\mathbf{u}^{\mathrm{b}} \cdot \nabla)\,\mathbf{u}^{\mathrm{b}}) = -\nabla\,\mathrm{p}^{\mathrm{b}} + \mu^{\mathrm{b}}\,\nabla^2\,\mathbf{u}^{\mathrm{b}} - \mathbf{g}\,\rho^{\mathrm{b}} \qquad z < \eta(x,y,t) \tag{3.9}$$

$$\nabla \cdot \mathbf{u}^{\mathrm{b}} = 0 \qquad z < \eta(x,y,t) \tag{3.10}$$

In order to consider lubrication effects we first non-dimensionalise the system. We also note that we will use subscript notation to indicate partial derivatives.

3.2.1 Non-dimensionalisation

For a typical lengthscale L (which for our purpose we define as diameter of the sphere $L = 2R(t)$), introduce a typical velocity U in the horizontal, and velocity W in the vertical. Then the horizontal x, y can be nondimensionalized with L, however the vertical height of the lubrication layer is expected to be significantly smaller than the vertical, so requre δL in the z direction, where $\delta \ll 1$. Letting $\bar{\cdot}$ denote non-dimensional variables, this gives the scalings:

$$x = L\bar{x}, \quad y = L\bar{y}, \quad z = \delta L\bar{z}, \quad \mathrm{u}^{\mathrm{a}} = U\,\bar{\mathrm{u}}^{\mathrm{a}}, \quad v = U\,\bar{\mathrm{v}}^{\mathrm{a}}, \quad \mathrm{w}^{\mathrm{a}} = W\,\bar{\mathrm{w}}^{\mathrm{a}}, \quad t = \frac{L}{U}\bar{t}. \tag{3.11}$$

When considering conservation of mass:

$$\begin{aligned} \nabla \cdot \mathbf{u}^{\mathrm{a}} &= 0 \\ \mathrm{u}^{\mathrm{a}}{}_x + \mathrm{v}^{\mathrm{a}}{}_y + \mathrm{v}^{\mathrm{a}}{}_z &= 0 \\ \frac{U}{L}\,\bar{\mathrm{u}}^{\mathrm{a}}{}_{\bar{x}} + \frac{U}{L}\,\bar{\mathrm{v}}^{\mathrm{a}}{}_{\bar{y}} + \frac{W}{\delta L}\,\bar{\mathrm{w}}^{\mathrm{a}}{}_{\bar{z}} &= 0 \end{aligned}$$

We expect the terms in the mass equation to balance, so we require the coefficients to match, giving

$$W = \delta U. \tag{3.12}$$

The non-dimensional conservation of mass equation is given by

$$\bar{\mathrm{u}}^{\mathrm{a}}{}_{\bar{x}} + \bar{\mathrm{v}}^{\mathrm{a}}{}_{\bar{y}} + \bar{\mathrm{w}}^{\mathrm{a}}{}_{\bar{z}} = 0 \tag{3.13}$$

Introducing this new scaling (3.12) into the conservation of momentum equations (3.3) for the air layer, we begin with the x-momentum equation.

$$\begin{aligned} \rho^{\mathrm{a}}(\mathrm{u}^{\mathrm{a}}{}_t + \mathrm{u}^{\mathrm{a}}\,\mathrm{u}^{\mathrm{a}}{}_x + \mathrm{v}^{\mathrm{a}}\,\mathrm{u}^{\mathrm{a}}{}_y + \mathrm{w}^{\mathrm{a}}\,\mathrm{u}^{\mathrm{a}}{}_z) &= -\,\mathrm{p}^{\mathrm{a}}{}_x + \mu^{\mathrm{a}}(\mathrm{u}^{\mathrm{a}}{}_{xx} + \mathrm{u}^{\mathrm{a}}{}_{yy} + \mathrm{u}^{\mathrm{a}}{}_{zz}) \\ \rho^{\mathrm{a}}\left(\frac{U}{L/U}\,\bar{\mathrm{u}}^{\mathrm{a}}{}_{\bar{t}} + U\,\bar{\mathrm{u}}^{\mathrm{a}}\,\frac{U}{L}\,\bar{\mathrm{u}}^{\mathrm{a}}{}_{\bar{x}} + U\,\bar{\mathrm{v}}^{\mathrm{a}}\,\frac{U}{L}\,\bar{\mathrm{u}}^{\mathrm{a}}{}_{\bar{y}} + \delta U\,\bar{\mathrm{w}}^{\mathrm{a}}\,\bar{\mathrm{u}}^{\mathrm{a}}{}_{z}\right) &= -\frac{1}{L}\,\mathrm{p}^{\mathrm{a}}{}_{\bar{x}} + \mu^{\mathrm{a}}(\frac{U}{L^2}\,\bar{\mathrm{u}}^{\mathrm{a}}{}_{\bar{x}\bar{x}} + \frac{U}{L^2}\,\bar{\mathrm{u}}^{\mathrm{a}}{}_{\bar{y}\bar{y}} + \frac{U}{\delta^2 L^2}\,\bar{\mathrm{u}}^{\mathrm{a}}{}_{\bar{z}\bar{z}}) \\ \frac{\rho^{\mathrm{a}}\,U^2}{L}\,(\bar{\mathrm{u}}^{\mathrm{a}}{}_{\bar{t}} + \bar{\mathrm{u}}^{\mathrm{a}}\,\bar{\mathrm{u}}^{\mathrm{a}}{}_{\bar{x}} + \bar{\mathrm{v}}^{\mathrm{a}}\,\bar{\mathrm{u}}^{\mathrm{a}}{}_{\bar{y}} + \bar{\mathrm{w}}^{\mathrm{a}}\,\bar{\mathrm{u}}^{\mathrm{a}}{}_{\bar{z}}) &= -\frac{1}{L}\,\mathrm{p}^{\mathrm{a}}{}_{\bar{x}} + \frac{\mu^{\mathrm{a}}\,U}{L^2}\left(\bar{\mathrm{u}}^{\mathrm{a}}{}_{\bar{x}\bar{x}} + \bar{\mathrm{v}}^{\mathrm{a}}{}_{\bar{y}\bar{y}} + \frac{1}{\delta^2}\,\bar{\mathrm{w}}^{\mathrm{a}}{}_{\bar{z}\bar{z}}\right) \end{aligned}$$

we now introduce a non-dimensional scaling for the pressure $\mathrm{p}^{\mathrm{a}} = P\,\bar{\mathrm{p}}^{\mathrm{a}}$. The pressure scaling must match with the largest term $\bar{\mathrm{u}}^{\mathrm{a}}{}_{\bar{z}\bar{z}}$. This gives $P = \frac{\mu^{\mathrm{a}} U}{L\delta^2}$. If we introduce the Reynolds number for the air layer as $\mathrm{Re}^{\mathrm{a}} = \frac{\mu^{\mathrm{a}}}{\rho^{\mathrm{a}} UL}$, we can write the x momentum equation as

$$\frac{D\,\bar{\mathrm{u}}^{\mathrm{a}}}{D\bar{t}} = \frac{-1}{\delta^2\,\mathrm{Re}^{\mathrm{a}}}\,\bar{\mathrm{p}}^{\mathrm{a}}{}_{\bar{x}} + \frac{1}{\mathrm{Re}^{\mathrm{a}}}(\bar{\mathrm{u}}^{\mathrm{a}}{}_{\bar{x}\bar{x}} + \bar{\mathrm{u}}^{\mathrm{a}}{}_{\bar{y}\bar{y}}) + \frac{1}{\delta^2\,\mathrm{Re}^{\mathrm{a}}}\,\bar{\mathrm{u}}^{\mathrm{a}}{}_{\bar{z}\bar{z}}$$

$$\delta^2\,\mathrm{Re}^{\mathrm{a}}\,\frac{D\,\bar{\mathrm{u}}^{\mathrm{a}}}{D\bar{t}} = -\,\bar{\mathrm{p}}^{\mathrm{a}}{}_{\bar{x}} + \delta^2(\bar{\mathrm{u}}^{\mathrm{a}}{}_{\bar{x}\bar{x}} + \bar{\mathrm{u}}^{\mathrm{a}}{}_{\bar{y}\bar{y}}) + \bar{\mathrm{u}}^{\mathrm{a}}{}_{\bar{z}\bar{z}} \tag{3.14}$$

Similarly, the y-momentum equation can be written

$$\delta^2\,\mathrm{Re}^{\mathrm{a}}\,\frac{D\,\bar{\mathrm{v}}^{\mathrm{a}}}{D\bar{t}} = -\,\bar{\mathrm{p}}^{\mathrm{a}}{}_{\bar{y}} + \delta^2(\bar{\mathrm{v}}^{\mathrm{a}}{}_{\bar{x}\bar{x}} + \bar{\mathrm{v}}^{\mathrm{a}}{}_{\bar{y}\bar{y}}) + \bar{\mathrm{v}}^{\mathrm{a}}{}_{\bar{z}\bar{z}} \tag{3.15}$$

However we consider the z-momentum equation separately, as there is less symmetry with the first two.

$$\rho^{\mathrm{a}}\left(\frac{\delta U}{L/U}\,\bar{\mathrm{w}}^{\mathrm{a}}{}_{\bar{t}} + U\,\bar{\mathrm{u}}^{\mathrm{a}}\,\frac{\delta U}{L}\,\bar{\mathrm{w}}^{\mathrm{a}}{}_{\bar{x}} + U\,\bar{\mathrm{v}}^{\mathrm{a}}\,\frac{\delta U}{L}\,\bar{\mathrm{w}}^{\mathrm{a}}{}_{\bar{y}} + \delta U\,\bar{\mathrm{w}}^{\mathrm{a}}\,\frac{\delta U}{\delta L}\,\bar{\mathrm{w}}^{\mathrm{a}}{}_{\bar{z}}\right)$$
$$= -\frac{\mu^{\mathrm{a}} U}{L\delta^2}\,\frac{1}{\delta L}\,\bar{\mathrm{p}}^{\mathrm{a}}{}_{\bar{z}} + \mu^{\mathrm{a}}\left(\frac{\delta U}{L^2}\,\bar{\mathrm{w}}^{\mathrm{a}}{}_{\bar{x}\bar{x}} + \frac{\delta U}{L^2}\,\bar{\mathrm{w}}^{\mathrm{a}}{}_{\bar{y}\bar{y}} + \frac{\delta U}{\delta^2 L^2}\,\bar{\mathrm{w}}^{\mathrm{a}}{}_{\bar{z}\bar{z}}\right) - g\,\rho^{\mathrm{a}}$$

$$\frac{\rho^{\mathrm{a}}\,\delta U^2}{L}\,(\bar{\mathrm{w}}^{\mathrm{a}}{}_{\bar{t}} + \bar{\mathrm{u}}^{\mathrm{a}}\,\bar{\mathrm{w}}^{\mathrm{a}}{}_{\bar{x}} + \bar{\mathrm{v}}^{\mathrm{a}}\,\bar{\mathrm{w}}^{\mathrm{a}}{}_{\bar{y}} + \bar{\mathrm{w}}^{\mathrm{a}}\,\bar{\mathrm{w}}^{\mathrm{a}}{}_{\bar{z}}) =$$
$$-\,\frac{\mu^{\mathrm{a}} U}{L^2\delta^3}\,\bar{\mathrm{p}}^{\mathrm{a}}{}_{\bar{z}} + \frac{\mu^{\mathrm{a}}\,\delta U}{L^2}\left(\bar{\mathrm{w}}^{\mathrm{a}}{}_{\bar{x}\bar{x}} + \bar{\mathrm{w}}^{\mathrm{a}}{}_{\bar{y}\bar{y}} + \frac{1}{\delta^2}\,\bar{\mathrm{w}}^{\mathrm{a}}{}_{\bar{z}\bar{z}}\right) - g\,\rho^{\mathrm{a}}$$

$$\frac{D\,\bar{\mathrm{w}}^{\mathrm{a}}}{D\bar{t}} = -\frac{\mu^{\mathrm{a}}}{\delta^4\,\rho^{\mathrm{a}} UL}\,\bar{\mathrm{p}}^{\mathrm{a}}{}_{\bar{z}} + \frac{\mu^{\mathrm{a}}}{\rho^{\mathrm{a}} UL}\left(\bar{\mathrm{w}}^{\mathrm{a}}{}_{\bar{x}\bar{x}} + \bar{\mathrm{w}}^{\mathrm{a}}{}_{\bar{y}\bar{y}} + \frac{1}{\delta^2}\,\bar{\mathrm{w}}^{\mathrm{a}}{}_{\bar{z}\bar{z}}\right) - \frac{gL}{\delta U^2}$$

Indroducing Re^{a} and multiplying through by $\mathrm{Re}^{\mathrm{a}}\,\delta^4$ gives the z-momentum equation.

$$\mathrm{Re}^{\mathrm{a}}\,\delta^4\,\frac{D\,\bar{\mathrm{w}}^{\mathrm{a}}}{D\bar{t}} = -\,\bar{\mathrm{p}}^{\mathrm{a}}{}_{\bar{z}} + \delta^4\,(\bar{\mathrm{w}}^{\mathrm{a}}{}_{\bar{x}\bar{x}} + \bar{\mathrm{w}}^{\mathrm{a}}{}_{\bar{y}\bar{y}}) + \delta^2\,\bar{\mathrm{w}}^{\mathrm{a}}{}_{\bar{z}\bar{z}} - \frac{g\,\rho^{\mathrm{a}}\,L^2\delta^3}{\mu^{\mathrm{a}}\,U} \tag{3.16}$$

Define $G = \frac{g\,\rho^{\mathrm{a}}\,L^2\delta^3}{\mu^{\mathrm{a}}\,U}$. If we say that $U = \mathcal{O}\left(\frac{\mu^{\mathrm{a}}}{g\,\rho^{\mathrm{a}}\,L^2\delta^3}\right)$ then $G = 1$.

Equations (3.14),(3.15),(3.16), when combined with (3.13), give the non-dimensional system of governing equations. If we now make lubrication theory assumptions, then we assume that $\delta \ll 1$ and furthermore $\mathrm{Re}^{\mathrm{a}}\,\delta^2 \ll 1$. Physically this is that the thickness/length aspect ratio is small

$$\frac{\delta L}{L} = \delta \ll 1,$$

and the reduced Reynolds number is small and intertial terms are much smaller than viscous terms, i.e

$$\frac{\rho^{\mathrm{a}}(\delta L)(\delta U)}{\mu^{\mathrm{a}}} = \delta^2\frac{\rho^{\mathrm{a}} UL}{\mu^{\mathrm{a}}} = \delta^2\,\mathrm{Re}^{\mathrm{a}} \ll 1$$

Then at leading order the governing equations are:

$$\bar{\mathrm{p}}^{\mathrm{a}}{}_{\bar{x}} = \bar{\mathrm{u}}^{\mathrm{a}}{}_{\bar{z}\bar{z}} \qquad \bar{\eta} \le z \le f \tag{3.17}$$

$$\bar{\mathrm{p}}^{\mathrm{a}}{}_{\bar{y}} = \bar{\mathrm{v}}^{\mathrm{a}}{}_{\bar{z}\bar{z}} \qquad \bar{\eta} \le z \le f \tag{3.18}$$

$$\bar{\mathrm{p}}^{\mathrm{a}}{}_{\bar{z}} = -1 \qquad \bar{\eta} \le z \le f \tag{3.19}$$

$$\bar{\mathrm{u}}^{\mathrm{a}}{}_{\bar{x}} + \bar{\mathrm{v}}^{\mathrm{a}}{}_{\bar{y}} + \bar{\mathrm{w}}^{\mathrm{a}}{}_{\bar{z}} = 0 \qquad \bar{\eta} \le z \le f \tag{3.20}$$

However it still remains to consider the boundary conditions at the free surface and the surface of the sphere. As we consider the perturbation on the free surface to be small, a reasonable

lengthscale of the perturbation is δL. i.e $\eta = \delta L \eta$.
On $z = \eta$ the domain is now $\bar{z} = \bar{\eta}$, and the kinematic condition becomes:

$$\begin{aligned} \eta_t + \mathrm{u}^{\mathrm{a}}\,\eta_x + \mathrm{v}^{\mathrm{a}}\,\eta_y &= \mathrm{w}^{\mathrm{a}} \\ \frac{\delta L}{L/U}\bar{\eta}_{\bar{t}} + U\,\bar{\mathrm{u}}^{\mathrm{a}}\,\frac{\delta L U}{L}\bar{\eta}_{\bar{x}} + U\,\bar{\mathrm{v}}^{\mathrm{a}}\,\frac{\delta L U}{L}\bar{\eta}_{\bar{y}} &= \delta U\,\bar{\mathrm{w}}^{\mathrm{a}} \\ \bar{\eta}_{\bar{t}} + \bar{\mathrm{u}}^{\mathrm{a}}\,\bar{\eta}_{\bar{x}} + \bar{\mathrm{v}}^{\mathrm{a}}\,\bar{\eta}_{\bar{y}} &= \bar{\mathrm{w}}^{\mathrm{a}} \end{aligned} \tag{3.21}$$

it remains unchanged in the non-dimensional case.
To consider the dynamic condition at this surface we need to first non-dimensionalise the stress tensors for each of the fluids σ^{a} and σ^{b} respectively. As they are derived from

$$\sigma_{i,j} = -p\delta_{i,j} + \mu[(u_i)_{x_j} + (u_j)_{x_i}]$$

for each respective fluid, we can non-dimensionalise elementwise to obtain:

$$\bar{\sigma^{\mathrm{a}}} = \frac{\mu^{\mathrm{a}}\,U}{L}\begin{pmatrix} \frac{-1}{\delta^2}\,\bar{\mathrm{p}}^{\mathrm{a}} + 2\,\bar{\mathrm{u}}^{\mathrm{a}}{}_{\bar{x}} & \bar{\mathrm{u}}^{\mathrm{a}}{}_{\bar{y}} + \bar{\mathrm{v}}^{\mathrm{a}}{}_{\bar{x}} & \frac{1}{\delta}\,\bar{\mathrm{u}}^{\mathrm{a}}{}_{\bar{z}} + \delta\,\bar{\mathrm{w}}^{\mathrm{a}}{}_{\bar{x}} \\ \bar{\mathrm{v}}^{\mathrm{a}}{}_{\bar{x}} + \bar{\mathrm{u}}^{\mathrm{a}}{}_{\bar{y}} & \frac{-1}{\delta^2}\,\bar{\mathrm{p}}^{\mathrm{a}} + 2\,\bar{\mathrm{v}}^{\mathrm{a}}{}_{\bar{y}} & \frac{1}{\delta}\,\bar{\mathrm{v}}^{\mathrm{a}}{}_{\bar{z}} + \delta\,\bar{\mathrm{w}}^{\mathrm{a}}{}_{\bar{y}} \\ \frac{1}{\delta}\,\bar{\mathrm{u}}^{\mathrm{a}}{}_{\bar{z}} + \delta\,\bar{\mathrm{w}}^{\mathrm{a}}{}_{\bar{x}} & \frac{1}{\delta}\,\bar{\mathrm{v}}^{\mathrm{a}}{}_{\bar{z}} + \delta\,\bar{\mathrm{w}}^{\mathrm{a}}{}_{\bar{y}} & \frac{-1}{\delta^2}\,\bar{\mathrm{p}}^{\mathrm{a}} + 2\,\bar{\mathrm{w}}^{\mathrm{a}}{}_{\bar{z}} \end{pmatrix} \tag{3.22}$$

$$\bar{\sigma^{\mathrm{b}}} = \rho^{\mathrm{b}}\,U^2\begin{pmatrix} -\bar{\mathrm{p}}^{\mathrm{b}} + \frac{2}{\mathrm{Re}^{\mathrm{b}}}\,\bar{\mathrm{u}}^{\mathrm{b}}{}_{\bar{x}} & \frac{1}{\mathrm{Re}^{\mathrm{b}}}\,\bar{\mathrm{u}}^{\mathrm{b}}{}_{\bar{y}} + \frac{1}{\mathrm{Re}^{\mathrm{b}}}\,\bar{\mathrm{v}}^{\mathrm{b}}{}_{\bar{x}} & \frac{1}{\mathrm{Re}^{\mathrm{b}}}\,\bar{\mathrm{u}}^{\mathrm{b}}{}_{\bar{z}} + \frac{1}{\mathrm{Re}^{\mathrm{b}}}\,\bar{\mathrm{w}}^{\mathrm{b}}{}_{\bar{x}} \\ \frac{1}{\mathrm{Re}^{\mathrm{b}}}\,\bar{\mathrm{v}}^{\mathrm{b}}{}_{\bar{x}} + \frac{1}{\mathrm{Re}^{\mathrm{b}}}\,\bar{\mathrm{u}}^{\mathrm{b}}{}_{\bar{y}} & -\bar{\mathrm{p}}^{\mathrm{b}} + \frac{2}{\mathrm{Re}^{\mathrm{b}}}\,\bar{\mathrm{v}}^{\mathrm{b}}{}_{\bar{y}} & \frac{1}{\mathrm{Re}^{\mathrm{b}}}\,\bar{\mathrm{v}}^{\mathrm{b}}{}_{\bar{z}} + \frac{1}{\mathrm{Re}^{\mathrm{b}}}\,\bar{\mathrm{w}}^{\mathrm{b}}{}_{\bar{y}} \\ \frac{1}{\mathrm{Re}^{\mathrm{b}}}\,\bar{\mathrm{u}}^{\mathrm{b}}{}_{\bar{z}} + \frac{1}{\mathrm{Re}^{\mathrm{b}}}\,\bar{\mathrm{w}}^{\mathrm{b}}{}_{\bar{x}} & \frac{1}{\mathrm{Re}^{\mathrm{b}}}\,\bar{\mathrm{v}}^{\mathrm{b}}{}_{\bar{z}} + \frac{1}{\mathrm{Re}^{\mathrm{b}}}\,\bar{\mathrm{w}}^{\mathrm{b}}{}_{\bar{y}} & -\bar{\mathrm{p}}^{\mathrm{b}} + \frac{2}{\mathrm{Re}^{\mathrm{b}}}\,\bar{\mathrm{w}}^{\mathrm{b}}{}_{\bar{z}} \end{pmatrix} \tag{3.23}$$

We also require the equations for the unit normal and tangential vectors:

$$\begin{aligned} \mathbf{n} &= [-\eta_x, -\eta_y, 1]/(1 + \eta_x^2 + \eta_y^2) \\ \mathbf{m}_x &= [1, 0, \eta_x]/(1 + \eta_x^2) \\ \mathbf{m}_y &= [0, 1, \eta_y]/(1 + \eta_y^2) \end{aligned}$$

This gives the non-dimensional vectors as:

$$\begin{aligned} \bar{\mathbf{n}} &= [-\delta\eta_x, -\delta\eta_y, 1]/(1 + \delta^2\eta_x^2 + \delta^2\eta_y^2) \\ \bar{\mathbf{m}}_x &= [1, 0, \delta\eta_x]/(1 + \delta^2\eta_x^2) \\ \bar{\mathbf{m}}_y &= [0, 1, \delta\eta_y]/(1 + \delta^2\eta_y^2) \end{aligned}$$

In order to balance the stress at the interface, there are three equations: one for the normal stress, and two for the orthogonal tangential stresses. We can work out the components individually. Starting with the air layer:

$$\begin{aligned} \bar{\mathbf{n}} \cdot \bar{\sigma^{\mathrm{a}}} \cdot \bar{\mathbf{n}} = \frac{\mu^{\mathrm{a}}\,U}{L(1 + \delta^2(\eta_x^2 + \eta_y^2))}\Bigg[& \left[\frac{-1}{\delta^2}\,\bar{\mathrm{p}}^{\mathrm{a}} + 2\,\bar{\mathrm{u}}^{\mathrm{a}}{}_{\bar{x}}\right]\bar{\eta}_{\bar{x}}^2\delta^2 + 2\left[\bar{\mathrm{u}}^{\mathrm{a}}{}_{\bar{y}} + \bar{\mathrm{v}}^{\mathrm{a}}{}_{\bar{x}}\right]\delta^2\bar{\eta}_{\bar{x}}\bar{\eta}_{\bar{y}} - 2\delta\left[\frac{1}{\delta}\,\bar{\mathrm{u}}^{\mathrm{a}}{}_{\bar{z}} + \delta\,\bar{\mathrm{w}}^{\mathrm{a}}{}_{\bar{x}}\right]\bar{\eta}_{\bar{x}} \\ & + \left[\frac{-1}{\delta^2}\,\bar{\mathrm{p}}^{\mathrm{a}} + 2\,\bar{\mathrm{v}}^{\mathrm{a}}{}_{\bar{y}}\right]\bar{\eta}_{\bar{x}}^2\delta^2 - 2\delta\left[\frac{1}{\delta}\,\bar{\mathrm{v}}^{\mathrm{a}}{}_{\bar{z}} + \delta\,\bar{\mathrm{w}}^{\mathrm{a}}{}_{\bar{y}}\right] + \left[\frac{-1}{\delta^2}\,\bar{\mathrm{p}}^{\mathrm{a}} + 2\,\bar{\mathrm{w}}^{\mathrm{a}}{}_{\bar{z}}\right]\Bigg] \\ = \frac{\mu^{\mathrm{a}}\,U}{L(1 + \delta^2(\eta_x^2 + \eta_y^2))}\Bigg[& -\bar{\mathrm{p}}^{\mathrm{a}}\,\bar{\eta}_{\bar{x}}^2 - \bar{\mathrm{p}}^{\mathrm{a}}\,\bar{\eta}_{\bar{y}}^2 - \frac{1}{\delta^2}\,\bar{\mathrm{p}}^{\mathrm{a}} - \bar{\mathrm{u}}^{\mathrm{a}}{}_{\bar{z}}\,\bar{\eta}_{\bar{x}} - \bar{\mathrm{v}}^{\mathrm{a}}{}_{\bar{z}}\,\bar{\eta}_{\bar{y}} + 2\,\bar{\mathrm{w}}^{\mathrm{a}}{}_{\bar{z}} + \mathcal{O}(\delta^2)\Bigg] \end{aligned}$$

$$\bar{\mathbf{m}}_x \cdot \bar{\sigma^{\mathrm{a}}} \cdot \bar{\mathbf{n}} = \frac{\mu^{\mathrm{a}} U}{L} \frac{1}{\sqrt{1+\delta^2(\eta_x^2+\eta_y^2)}} \frac{1}{\sqrt{1+\delta^2\bar{\eta}_{\bar{x}}^2}} \Bigg[-\delta \left[\frac{-1}{\delta^2}\, \bar{\mathrm{p}}^{\mathrm{a}} + 2\, \bar{\mathrm{u}}^{\mathrm{a}}{}_{\bar{x}} \right] \bar{\eta}_{\bar{x}} - \delta \left[\bar{\mathrm{u}}^{\mathrm{a}}{}_{\bar{y}} + \bar{\mathrm{v}}^{\mathrm{a}}{}_{\bar{x}} \right] \bar{\eta}_{\bar{y}}$$
$$+ \left[\frac{1}{\delta}\, \bar{\mathrm{u}}^{\mathrm{a}}{}_{\bar{z}} + \delta\, \bar{\mathrm{w}}^{\mathrm{a}}{}_{\bar{x}} \right] (1+\delta^2\bar{\eta}_{\bar{x}}^2) + \left[\frac{1}{\delta}\, \bar{\mathrm{v}}^{\mathrm{a}}{}_{\bar{z}} + \delta\, \bar{\mathrm{w}}^{\mathrm{a}}{}_{\bar{y}} \right] \delta^2 \bar{\eta}_{\bar{y}} \bar{\eta}_{\bar{x}} + \delta \left[\frac{1}{\delta}\, \bar{\mathrm{p}}^{\mathrm{a}} + 2\, \bar{\mathrm{w}}^{\mathrm{a}}{}_{\bar{z}} \right] \bar{\eta}_{\bar{x}} \Bigg]$$
$$= \frac{\mu^{\mathrm{a}} U}{L} \frac{1}{\sqrt{1+\delta^2(\eta_x^2+\eta_y^2)}} \frac{1}{\sqrt{1+\delta^2\bar{\eta}_{\bar{x}}^2}} \left[\frac{1}{\delta}\, \bar{\mathrm{u}}^{\mathrm{a}}{}_{\bar{z}} + \mathcal{O}(\delta^2) \right]$$

Similarly for $\bar{\mathbf{m}}_y$

$$\bar{\mathbf{m}}_y \cdot \bar{\sigma^{\mathrm{a}}} \cdot \bar{\mathbf{n}} \frac{\mu^{\mathrm{a}} U}{L} \frac{1}{\sqrt{1+\delta^2(\eta_x^2+\eta_y^2)}} \frac{1}{\sqrt{1+\delta^2\bar{\eta}_{\bar{y}}^2}} \left[\frac{1}{\delta}\, \bar{\mathrm{v}}^{\mathrm{a}}{}_{\bar{z}} + \mathcal{O}(\delta^2) \right]$$

Looking now at the fluid regime:

$$\bar{\mathbf{n}} \cdot \bar{\sigma^{\mathrm{b}}} \cdot \bar{\mathbf{n}} = \frac{\rho^{\mathrm{b}} U^2}{1+\delta^2(\bar{\eta}_{\bar{x}}^2+\bar{\eta}_{\bar{y}}^2)} \Bigg[\delta^2 \left[-\bar{\mathrm{p}}^{\mathrm{b}} + \frac{2}{\mathrm{Re}^{\mathrm{b}}}\, \bar{\mathrm{u}}^{\mathrm{b}}{}_{\bar{x}} \right] \bar{\eta}_{\bar{x}}^2 + 2\delta^2 \left[\frac{1}{\mathrm{Re}^{\mathrm{b}}}\, \bar{\mathrm{u}}^{\mathrm{b}}{}_{\bar{y}} + \frac{1}{\mathrm{Re}^{\mathrm{b}}}\, \bar{\mathrm{v}}^{\mathrm{b}}{}_{\bar{x}} \right] \bar{\eta}_{\bar{x}} \bar{\eta}_{\bar{y}}$$
$$- 2\delta \left[\frac{1}{\mathrm{Re}^{\mathrm{b}}}\, \bar{\mathrm{u}}^{\mathrm{b}}{}_{\bar{z}} + \frac{1}{\mathrm{Re}^{\mathrm{b}}}\, \bar{\mathrm{w}}^{\mathrm{b}}{}_{\bar{x}} \right] \bar{\eta}_{\bar{x}} + \delta^2 \left[-\bar{\mathrm{p}}^{\mathrm{b}} + \frac{2}{\mathrm{Re}^{\mathrm{b}}}\, \bar{\mathrm{v}}^{\mathrm{b}}{}_{\bar{y}} \right] \bar{\eta}_{\bar{y}}^2$$
$$- 2\delta \left[\frac{1}{\mathrm{Re}^{\mathrm{b}}}\, \bar{\mathrm{v}}^{\mathrm{b}}{}_{\bar{z}} + \frac{1}{\mathrm{Re}^{\mathrm{b}}}\, \bar{\mathrm{w}}^{\mathrm{b}}{}_{\bar{y}} \right] \bar{\eta}_{\bar{y}} + \left[-\bar{\mathrm{p}}^{\mathrm{b}} + \frac{2}{\mathrm{Re}^{\mathrm{b}}}\, \bar{\mathrm{w}}^{\mathrm{b}}{}_{\bar{z}} \right] \Bigg]$$
$$= \frac{\rho^{\mathrm{b}} U^2}{1+\delta^2(\bar{\eta}_{\bar{x}}^2+\bar{\eta}_{\bar{y}}^2)} \left[-\bar{\mathrm{p}}^{\mathrm{b}} + \frac{2}{\mathrm{Re}^{\mathrm{b}}}\, \bar{\mathrm{w}}^{\mathrm{b}}{}_{\bar{z}} + \mathcal{O}(\delta) \right]$$

$$\bar{\mathbf{m}}_x \cdot \bar{\sigma^{\mathrm{b}}} \cdot \bar{\mathbf{n}} = \frac{\rho^{\mathrm{b}} U^2}{\sqrt{1+\delta^2(\eta_x^2+\eta_y^2)}} \frac{1}{\sqrt{1+\delta^2\bar{\eta}_{\bar{x}}^2}} \Bigg[-\delta \left[-\bar{\mathrm{p}}^{\mathrm{b}} + \frac{2}{\mathrm{Re}^{\mathrm{b}}}\, \bar{\mathrm{u}}^{\mathrm{b}}{}_{\bar{x}} \right] \bar{\eta}_{\bar{x}}$$
$$- \delta \left[\frac{1}{\mathrm{Re}^{\mathrm{b}}}\, \bar{\mathrm{u}}^{\mathrm{b}}{}_{\bar{y}} + \frac{1}{\mathrm{Re}^{\mathrm{b}}}\, \bar{\mathrm{v}}^{\mathrm{b}}{}_{\bar{x}} \right] \bar{\eta}_{\bar{y}} + \left[\frac{1}{\mathrm{Re}^{\mathrm{b}}}\, \bar{\mathrm{u}}^{\mathrm{b}}{}_{\bar{z}} + \frac{1}{\mathrm{Re}^{\mathrm{b}}}\, \bar{\mathrm{w}}^{\mathrm{b}}{}_{\bar{x}} \right] (1+\delta^2\bar{\eta}_{\bar{x}}^2)$$
$$+ \left[\bar{\mathrm{v}}^{\mathrm{b}}{}_{\bar{z}} + \bar{\mathrm{w}}^{\mathrm{b}}{}_{\bar{y}} \right] \delta^2 \bar{\eta}_{\bar{y}} \bar{\eta}_{\bar{x}} + \delta \left[-\bar{\mathrm{p}}^{\mathrm{b}} + \frac{2}{\mathrm{Re}^{\mathrm{b}}}\, \bar{\mathrm{w}}^{\mathrm{b}}{}_{\bar{z}} \right] \bar{\eta}_{\bar{x}} \Bigg]$$
$$= \frac{\rho^{\mathrm{b}} U^2}{\sqrt{1+\delta^2(\eta_x^2+\eta_y^2)}} \frac{1}{\sqrt{1+\delta^2\bar{\eta}_{\bar{x}}^2}} \left[\frac{1}{\mathrm{Re}^{\mathrm{b}}}\, \bar{\mathrm{u}}^{\mathrm{b}}{}_{\bar{z}} + \frac{1}{\mathrm{Re}^{\mathrm{b}}}\, \bar{\mathrm{w}}^{\mathrm{b}}{}_{\bar{x}} + \mathcal{O}(\delta) \right]$$

$$\bar{\mathbf{m}}_y \cdot \bar{\sigma^{\mathrm{b}}} \cdot \bar{\mathbf{n}} = \frac{\rho^{\mathrm{b}} U^2}{\sqrt{1+\delta^2(\eta_x^2+\eta_y^2)}} \frac{1}{\sqrt{1+\delta^2\bar{\eta}_{\bar{y}}^2}} \left[\frac{1}{\mathrm{Re}^{\mathrm{b}}}\, \bar{\mathrm{v}}^{\mathrm{b}}{}_{\bar{z}} + \frac{1}{\mathrm{Re}^{\mathrm{b}}}\, \bar{\mathrm{w}}^{\mathrm{b}}{}_{\bar{y}} + \mathcal{O}(\delta) \right]$$

So the stress balances become

$$\rho^{\mathrm{b}} U^2 \left[-\bar{\mathrm{p}}^{\mathrm{b}} + \frac{2}{\mathrm{Re}^{\mathrm{b}}}\, \bar{\mathrm{w}}^{\mathrm{b}}{}_{\bar{z}} \right] - \frac{\mu^{\mathrm{a}} U}{L} \left[\frac{-1}{\delta^2}\, \bar{\mathrm{p}}^{\mathrm{a}} \right] = \sigma(\nabla \cdot \mathbf{n}) + \mathcal{O}(\delta^2) \tag{3.24}$$

$$\rho^{\mathrm{b}} U^2 \left(\frac{1}{\mathrm{Re}^{\mathrm{b}}}\, \bar{\mathrm{u}}^{\mathrm{b}}{}_{\bar{z}} + \frac{1}{\mathrm{Re}^{\mathrm{b}}}\, \bar{\mathrm{w}}^{\mathrm{b}}{}_{\bar{x}} \right) = \frac{\mu^{\mathrm{a}}}{\delta} (\bar{\mathrm{u}}^{\mathrm{a}}{}_{\bar{z}}) + \mathcal{O}(\delta) \tag{3.25}$$

$$\rho^{\mathrm{b}} U^2 \left(\frac{1}{\mathrm{Re}^{\mathrm{b}}}\, \bar{\mathrm{v}}^{\mathrm{b}}{}_{\bar{z}} + \frac{1}{\mathrm{Re}^{\mathrm{b}}}\, \bar{\mathrm{w}}^{\mathrm{b}}{}_{\bar{y}} \right) = \frac{\mu^{\mathrm{a}}}{\delta} (\bar{\mathrm{v}}^{\mathrm{a}}{}_{\bar{z}}) + \mathcal{O}(\delta) \tag{3.26}$$

So we now have the full system in non-dimensional form,(3.17)-(3.20), (3.21),and (3.24)-(3.26) .

3.2.2 Deriving the lubrication equations

We drop the barred ($\bar{u}$) notation but remain in the non-dimensional state for the remainder of this chapter.

In the governing equations (3.14) - (3.16) there is no inclusion of $\mathrm{w^a}$, so rather than require determining it, we can use (3.13) to eliminate the need of it. We integrate the conservation of mass equation over the domain of the air layer $\eta < z < f$.

$$\begin{aligned} \mathrm{u^a}_x + \mathrm{v^a}_y + \mathrm{w^a}_z &= 0 \\ \int_\eta^f (\mathrm{u^a}_x + \mathrm{v^a}_y + \mathrm{w^a}_z)\, dz &= 0 \\ \int_\eta^f (\mathrm{u^a}_x + \mathrm{v^a}_y)\, dz + \mathrm{w^a}\,|_f - \mathrm{w^a}\,|_\eta &= 0 \end{aligned}$$

Here we apply Leibnitz integral rule over $\mathrm{u^a}_x$ and $\mathrm{v^a}_y$. We have that $\mathrm{w^a}$ perscribed at f is given by the no-slip boundary condition on the sphere, and $\mathrm{w^a}$ at η is given by the kinematic condition on the free surface, which we are looking to make the subject of the equation.

$$\mathrm{w^a}\,\big|_{z=\eta} = \int_\eta^f \mathrm{u^a}_x\, dz + \int_\eta^f \mathrm{v^a}_x\, dz + W_0.$$

Leibniz integral rule: $\left(\int_{p(x)}^{q(x)} \gamma(x,t)dt\right)_x = \gamma\big|_q q_x - \gamma\big|_p p_x + \int_{p(x)}^{q(x)} \gamma_x dt$. Thus

$$\begin{aligned} \int_\eta^f \mathrm{u^a}_x\, dz &= \left(\int_\eta^f \mathrm{u^a}\, dz\right)_x + \mathrm{u^a}\,\big|_\eta \eta_x - \mathrm{u^a}\,|_f f_x, \\ \int_\eta^f \mathrm{v^a}_y\, dz &= \left(\int_\eta^f \mathrm{v^a}\, dz\right)_y + \mathrm{v^a}\,\big|_\eta \eta_y - \mathrm{v^a}\,|_f f_y. \end{aligned}$$

On the surface of the sphere $z = f$, $\mathrm{u^a} = U_0$ and $\mathrm{v^a} = V_0$ due to the matching condition. Hence substituting these definitions of the integrals into the kinematic boundary condition gives

$$\begin{aligned} &\eta_t + \mathrm{u^a}\,\eta_x + \mathrm{v^a}\,\eta_y = w, \\ &\eta_t + \mathrm{u^a}\,\eta_x + \mathrm{v^a}\,\eta_y = \left(\int_\eta^f \mathrm{u^a}\, dz\right)_x + \mathrm{u^a}\,\big|_\eta \eta_x - \mathrm{u^a}\,|_f f_x + \left(\int_\eta^f \mathrm{v^a}\, dz\right)_y + \mathrm{v^a}\,\big|_\eta \eta_y - \mathrm{v^a}\,|_f f_y + W_0, \\ &\eta_t = \left(\int_\eta^f \mathrm{u^a}\, dz\right)_x + \left(\int_\eta^f \mathrm{v^a}\, dz\right)_y - U_0 f_x - V_0 f_y + W_0. \end{aligned} \tag{3.27}$$

It remains to determine the integrals, which can be done using (3.17) - (3.20). From the z-momentum equation (3.19), we have the pressure must be given by

$$\mathrm{p^a} = p_0(x,y,t) - z$$

for some function p_0 to still be determined. However this means that the x and y derivatives of $\mathrm{p^a}$ are given by $(p_0)_x$ and $(p_0)_y$ respectively, so are independent of z. Then we can integrate the x and y momentum equations twice with respect to z to obtain

$$\begin{aligned} \mathrm{u^a} &= \frac{\mathrm{p^a}_x\, z^2}{2} + Az + B, \\ \mathrm{v^a} &= \frac{\mathrm{p^a}_y\, z^2}{2} + Cz + D. \end{aligned}$$

We can use the no-slip condition on the surface $z = f$ to determine B and D:

$$\begin{aligned}
\mathrm{u}^{\mathrm{a}} &= \frac{\mathrm{p}^{\mathrm{a}}{}_x (z^2 - f^2)}{2} + A(z - f) + U_0, \\
\mathrm{v}^{\mathrm{a}} &= \frac{\mathrm{p}^{\mathrm{a}}{}_y (z^2 - f^2)}{2} + C(z - f) + V_0.
\end{aligned}$$

It remains to determine A and C, which can be done by considering the dynamic condition (stress balancing) on the surface $z = \eta$. We can use (3.25) and (3.26), with taking $\mathrm{u}^{\mathrm{a}} = \mathrm{p}^{\mathrm{a}}{}_x \, \eta + A$ and $\mathrm{v}^{\mathrm{a}} = \mathrm{p}^{\mathrm{a}}{}_y \, \eta + C$.

$$\begin{aligned}
\rho^{\mathrm{b}} U^2 \left(\frac{1}{\mathrm{Re}^{\mathrm{b}}} \, \mathrm{u}^{\mathrm{b}}{}_z + \frac{1}{\mathrm{Re}^{\mathrm{b}}} \, \mathrm{w}^{\mathrm{b}}{}_x\right) &= \frac{\mu^{\mathrm{a}}}{\delta} (\mathrm{p}^{\mathrm{a}}{}_x \, \eta + A) \\
A &= \left[\frac{\rho^{\mathrm{b}} U^2}{\mathrm{Re}^{\mathrm{b}}} (\mathrm{u}^{\mathrm{b}}{}_z + \mathrm{w}^{\mathrm{b}}{}_x) - \frac{\mu^{\mathrm{a}}}{\delta} \, \mathrm{p}^{\mathrm{a}}{}_x \, \eta\right] \frac{\delta}{\mu^{\mathrm{a}}}
\end{aligned}$$

and similarly

$$\begin{aligned}
\rho^{\mathrm{b}} U^2 \left(\frac{1}{\mathrm{Re}^{\mathrm{b}}} \, \mathrm{v}^{\mathrm{b}}{}_z + \frac{1}{\mathrm{Re}^{\mathrm{b}}} \, \mathrm{w}^{\mathrm{b}}{}_y\right) &= \frac{\mu^{\mathrm{a}}}{\delta} (\mathrm{p}^{\mathrm{a}}{}_y \, \eta + C) \\
C &= \left[\frac{\rho^{\mathrm{b}} U^2}{\mathrm{Re}^{\mathrm{b}}} (\mathrm{v}^{\mathrm{b}}{}_z + \mathrm{w}^{\mathrm{b}}{}_x) - \frac{\mu^{\mathrm{a}}}{\delta} \, \mathrm{p}^{\mathrm{a}}{}_y \, \eta\right] \frac{\delta}{\mu^{\mathrm{a}}}
\end{aligned}$$

this gives the forms of u^{a} and v^{a}

$$\mathrm{u}^{\mathrm{a}} = \mathrm{p}^{\mathrm{a}}{}_x \, \frac{(z^2 - f^2)}{2} - \mathrm{p}^{\mathrm{a}}{}_x \, \eta(z - f) + \frac{\delta \, \rho^{\mathrm{b}} U^2}{\mu^{\mathrm{a}} \, \mathrm{Re}^{\mathrm{b}}} (\mathrm{u}^{\mathrm{b}}{}_z + \mathrm{w}^{\mathrm{b}}{}_x)(z - f) + U_0 \tag{3.28}$$

$$\mathrm{v}^{\mathrm{a}} = \mathrm{p}^{\mathrm{a}}{}_y \, \frac{(z^2 - f^2)}{2} - \mathrm{p}^{\mathrm{a}}{}_y \, \eta(z - f) + \frac{\delta \, \rho^{\mathrm{b}} U^2}{\mu^{\mathrm{a}} \, \mathrm{Re}^{\mathrm{b}}} (\mathrm{v}^{\mathrm{b}}{}_z + \mathrm{w}^{\mathrm{b}}{}_y)(z - f) + V_0 \tag{3.29}$$

We can now derive the explicit form of the integrals required within the kinematic boundary condition:

$$\begin{aligned}
\int_\eta^f \mathrm{u}^{\mathrm{a}} \, dz &= \int_\eta^f \mathrm{p}^{\mathrm{a}}{}_x \left(\frac{(z^2 - f^2)}{2} - \eta(z - f)\right) + \frac{\delta \, \rho^{\mathrm{b}} U^2}{\mu^{\mathrm{a}} \, \mathrm{Re}^{\mathrm{b}}} (\mathrm{u}^{\mathrm{b}}{}_z + \mathrm{w}^{\mathrm{b}}{}_x)(z - f) + U_0 \, dx \\
&= \left(\mathrm{p}^{\mathrm{a}}{}_x \left[\frac{z^3}{6} - \frac{f^2 z}{2} - \frac{\eta z^2}{2} + \eta f z - \frac{\eta z^2}{2} + \eta f z\right] + \frac{\rho^{\mathrm{b}} U^2}{\mathrm{Re}^{\mathrm{b}}} (\mathrm{u}^{\mathrm{b}}{}_z + \mathrm{w}^{\mathrm{b}}{}_x) \left[\frac{z^2}{2} - z f\right] + U_0 z\right) \Bigg|_\eta^f \\
&= \mathrm{p}^{\mathrm{a}}{}_x \, \frac{(\eta - f)^3}{3} + \frac{\delta \, \rho^{\mathrm{b}} U^2}{\mu^{\mathrm{a}} \, \mathrm{Re}^{\mathrm{b}}} (\mathrm{u}^{\mathrm{b}}{}_z + \mathrm{w}^{\mathrm{b}}{}_x) \frac{(\eta - f)^2}{2} - U_0 (\eta - f)
\end{aligned}$$

with similar for the integral for v^{a}

$$\int_\eta^f \mathrm{v}^{\mathrm{a}} \, dz = \mathrm{p}^{\mathrm{a}}{}_y \, \frac{(\eta - f)^3}{3} + \frac{\delta \, \rho^{\mathrm{b}} U^2}{\mu^{\mathrm{a}} \, \mathrm{Re}^{\mathrm{b}}} (\mathrm{v}^{\mathrm{b}}{}_z + \mathrm{w}^{\mathrm{b}}{}_y) \frac{(\eta - f)^2}{2} - V_0 (\eta - f)$$

This gives the kinematic boundary condition in terms of p as

$$\begin{aligned}
\eta_t = &\left[\mathrm{p}^{\mathrm{a}}{}_x \, \frac{(\eta - f)^3}{3} + \frac{\delta \, \rho^{\mathrm{b}} U^2}{\mu^{\mathrm{a}} \, \mathrm{Re}^{\mathrm{b}}} (\mathrm{u}^{\mathrm{b}}{}_z + \mathrm{w}^{\mathrm{b}}{}_x) \frac{(\eta - f)^2}{2} - U_0 (\eta - f)\right]_x \\
&+ \left[\mathrm{p}^{\mathrm{a}}{}_y \, \frac{(\eta - f)^3}{3} + \frac{\delta \, \rho^{\mathrm{b}} U^2}{\mu^{\mathrm{a}} \, \mathrm{Re}^{\mathrm{b}}} (\mathrm{v}^{\mathrm{b}}{}_z + \mathrm{w}^{\mathrm{b}}{}_y) \frac{(\eta - f)^2}{2} - V_0 (\eta - f)\right]_y \\
&- U_0 f_x - V_0 f_y + W_0
\end{aligned} \tag{3.30}$$

We can determine what should replace p_x and p_y from the normal stress equation (3.24).

$$\begin{aligned}
\rho^{\mathrm{b}} U^2 \left[-\mathrm{p}^{\mathrm{a}} + \frac{2}{\mathrm{Re}^{\mathrm{b}}} \mathrm{w}^{\mathrm{b}}{}_z \right] - \frac{\mu^{\mathrm{a}} U}{L} \left[\frac{-1}{\delta^2} \mathrm{p}^{\mathrm{a}} \right] &= \sigma(\nabla \cdot \mathbf{n}) + \mathcal{O}(\delta^2) \\
\frac{\mu^{\mathrm{a}} U}{L\delta^2} \mathrm{p}^{\mathrm{a}} &= \rho^{\mathrm{b}} U^2 \left[-\mathrm{p}^{\mathrm{b}} + \frac{2}{\mathrm{Re}^{\mathrm{b}}} \mathrm{w}^{\mathrm{b}}{}_z \right] - \sigma(\nabla \cdot \mathbf{n}) \\
\mathrm{p}^{\mathrm{a}} &= \frac{\delta^2 L \rho^{\mathrm{b}} U}{\mu^{\mathrm{a}}} \left[-\mathrm{p}^{\mathrm{b}} + \frac{2}{\mathrm{Re}} \mathrm{w}^{\mathrm{b}}{}_z \right] - \frac{L\delta^2}{\mu^{\mathrm{a}} U} \sigma(\nabla \cdot \mathbf{n}) \\
\mathrm{p}^{\mathrm{a}} &= \frac{\delta^2 L \rho^{\mathrm{b}} U}{\mu^{\mathrm{a}}} \left[-\mathrm{p}^{\mathrm{b}} + \frac{2}{\mathrm{Re}} \mathrm{w}^{\mathrm{b}}{}_z \right] - \frac{L\delta^2}{\mu^{\mathrm{a}} U} \frac{\delta L}{L^2} \sigma(\Delta\eta) \\
\mathrm{p}^{\mathrm{a}} &= \frac{\delta^2 L \rho^{\mathrm{b}} U}{\mu^{\mathrm{a}}} \left[-\mathrm{p}^{\mathrm{b}} + \frac{2}{\mathrm{Re}} \mathrm{w}^{\mathrm{b}}{}_z \right] - \frac{\delta^3}{\mu^{\mathrm{a}} U} \sigma(\Delta\eta)
\end{aligned}$$

this equation for the pressure can then be coupled with equation (3.30)

$$\mathrm{p}^{\mathrm{a}} = \alpha\, \sigma^{\mathrm{b}}{}_{3,3} - \beta\sigma(\Delta\eta), \tag{3.31}$$

$$\eta_t = \mathbf{U}_{\mathrm{sphere}} \cdot \mathbf{n}_{\mathrm{sphere}} + \nabla_H \cdot \left[(\nabla_H \cdot \mathrm{p}^{\mathrm{a}}) \frac{(\eta - f)^3}{3} + \gamma(\sigma^{\mathrm{b}}{}_{3,1}, \sigma^{\mathrm{b}}{}_{3,2}) \frac{(\eta - f)^2}{2} - \mathbf{U}_{\mathrm{sphere}_H} (\eta - f) \right], \tag{3.32}$$

where ∇_H is the horizontal gradient vector, $\mathbf{n}_{\mathrm{sphere}}$ is the outward normal to the sphere, and we've introduced the coefficients

$$\alpha = \frac{\delta^2 L \rho^{\mathrm{b}} U}{\mu^{\mathrm{a}}}, \qquad \beta = \frac{\delta^2}{\mu^{\mathrm{a}} U}, \qquad \gamma = \frac{\delta}{\mu^{\mathrm{a}}}.$$

It will be discussed in the next chapter how we plan on expanding on these equations. We will also discuss how (3.31) and (3.32) combine with the work done in chapter 2 to study the coupled system of air and fluid.

4 Future Work

4.1 Avenues of future research

The work within the previous chapters of this report is an overview, or introduction, to the area of study that will undertaken within the next three years. In Chapter 2 the global problem of droplets walking on a vibrating bath was explained, and a numerical solver for the evolution of a free surface of a vibrating bath under a periodic pressure forcing was developed. The code has been constructed in such a way that improvements and developments to the equations, and the code itself can be easily implemented. It will act as a basis for the rest of the proposed work spoken about later in this chapter. In Chapter 3 for a sufficiently small height $h(t)$ between the bath and the hydrophobic sphere,lubrication theory was used to derive a coupled system of equations that outputs the pressure term of the air layer.

As such there are some potential avenues of future work laid out in the rest of this chapter.

4.1.1 Improvement of Lubrication Theory

The most immediate progression of the work presented thus far, is expanding the lubrication model developed in Chapter 3 to replace the hydrophobic sphere with a droplet of the same fluid as the bath. This will require replacing the no-flux and no-slip conditons on the boundary $z = f$ with a kinematic boundary condition and a stress balancing condition. Namely by considering the fluid within the droplet denoted by a superscript d, $\cdot^d$, and its velocity as $\mathbf{u}^{\mathrm{d}} = (\mathrm{u}^{\mathrm{d}}, \mathrm{v}^{\mathrm{d}}, \mathrm{w}^{\mathrm{d}})$ on the boundary $z = f(x, y, t)$ which is now the interface between the droplet and the air layer $\mathbf{u}^{\mathrm{a}}$, we have the boundary conditions

$$\begin{aligned}
f_t + \mathbf{u}^{\mathrm{a}} \cdot \nabla(f - z) = 0 \qquad & z = f(x, y, t) \\
\mathbf{n}^s \cdot \sigma^{\mathrm{d}} \cdot \mathbf{n}^s - \mathbf{n}^s \cdot \sigma^{\mathrm{a}} \cdot \mathbf{n}^s = \sigma(\nabla \cdot \mathbf{n}^s) \qquad & z = f(x, y, t) \\
\mathbf{m}_x^s \cdot \sigma^{\mathrm{d}} \cdot \mathbf{n}^s - \mathbf{m}_x^s \cdot \sigma^{\mathrm{a}} \cdot \mathbf{n}^s = 0 \qquad & z = f(x, y, t) \\
\mathbf{m}_y^s \cdot \sigma^{\mathrm{d}} \cdot \mathbf{n}^s - \mathbf{m}_y^s \cdot \sigma^{\mathrm{a}} \cdot \mathbf{n}^s = 0 \qquad & z = f(x, y, t)
\end{aligned}$$

where $\mathbf{n}^s, \mathbf{m}_x^s, \mathbf{m}_y^s$ are the unit normal and tangential vectors to the surface $f(x, y, t)$.

With this inclusion we will have a complete model of an air lubrication layer between two fluids, however the physical geometries within the droplet dynamics are still not fully considered. The lubrication layer only takes effect within a small area beneath the droplet whilst at its lowest point in flight. We currently don't have a model for what happens on the edge of this area, where the fluid bath starts to pull away from the droplet and stuface tension effects take place. From Figure 10 we can see frames from the results of numerical simulations ran by Cimpeanu [11]. The central photo depicts the lowest point of flight, when the lubrication layer is widest , and there is an area where the pressure balances out again as the air layer widens out and meets the rest of the air. Perhaps more interesting though is what occurs in the first and last pictures in this trio. These depict the pressure at initial impact and at lift-off and there is a clear 'jet-stream' of high pressure being forced out, and low pressure beign pulled in respectively. How these interplay with the model of the lubrication layer we have yet to determine. Though they do raise the question of when do lubrication effects start to dominate and when to start using the lubrication model.

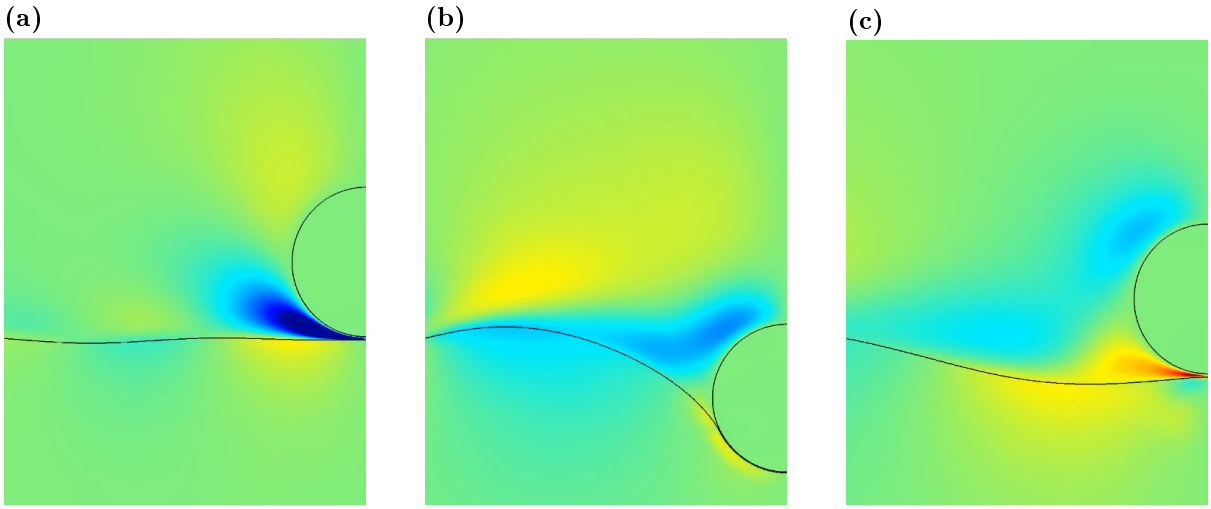

Figure 10: Included with permission from R. Cimpeanu [11, 3]. Numerical results from solving the full Navier-Stokes for the axiymmetric system of a solid sphere impacting on a bath. Colour indicates pressure, with dark blue indicating areas of high pressure and red indicating areas of low pressure. (a) is just before impact, (b) during contact at the lowest point of the droplets motion, and (c) just after liftoff.

4.1.2 Full flight

The lubrication theory model only applies when the height of the air layer is sufficiently small. As the droplet bounces, there is a point in time when there is a tiny area within this height requirement, and as the droplet continues to fall the area that can be modelled with lubrication theory increases. How and when we model the start of the lubrication effects will need to be determined.

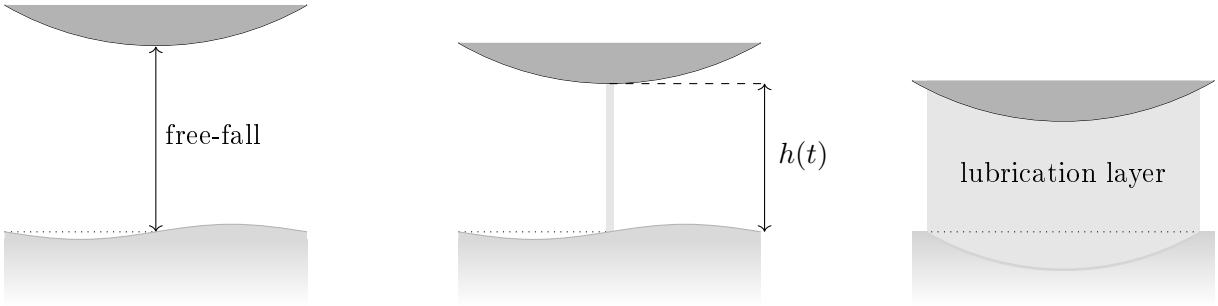

Figure 11: Different heights of sphere demonstrating how the lubrication layer starts as a fixed point that expands out with an effective radius $r(t)$.

Work done by Durey & Milewski [7], and Milewski et al [15] eradicate this problem by considering impact as instantaneous. This was validated by experimental data, shown in Figure 12. The time within the impact phase - from first contact to largest effective radius is near instantaneous, whereas the contact and liftoff phases take significantly longer.

As such we also used this idea of quick impact in Chapter 2 when developing a forcing term for the pressure of our numerical 'droplet'. We assumed that impact was instant resulting in a sharp spike of pressure, then a gradual release of pressure as the droplet was forced upwards by the resolving surface tension of the bath until the pressure on the bath was zero at the time of liftoff.

We want to replace this instantaneous impact by considering the lubrication layer within an oscillating domain. The domain would vanish whilst the droplet is in free flight, form as a singular point once the droplet is within a sufficient height range and then grows out with an 'effective radius $R(t)$', before reaching a maxiumum radius and then peeling off during liftoff.

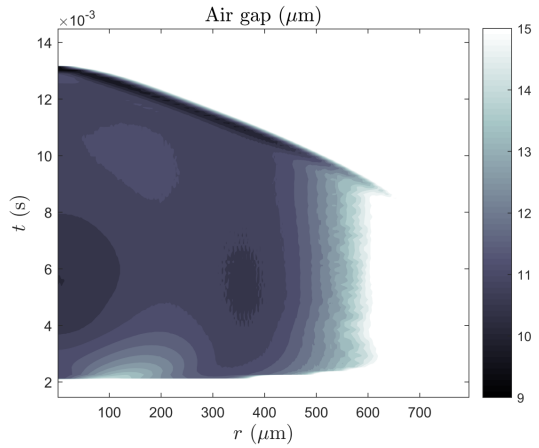

Figure 12: Included with permission from R. Cimpeanu [3]. Colour gradient represents air layer (μm) thickness over the radius (μm) along the horizontal. Progression in time (ms) is up the vertical axis. Graph can be separated into three stages, 'impact' happening very quickly around $t \approx 2.4\text{e}^{-3}$, then a quasi-steady 'contact' phase where the droplet and bath move together from $t \approx 3\text{e}^{-3}$ to $t \approx 10\text{e}^{-3}$, and finally a 'liftoff' phase where the bath appears to slowly peel away from the droplet.

This 'oscillating domain' feels more true to the physical action the droplet takes and follows the sketched motion as in Figure 11. The issue with this is how to consider that first singularity, as issues of singularities may arise either numerically or asymptotically.

4.1.3 Walkers

Walking droplets arise when the vibration of the Faraday forcing is iclose to the Faraday threshold, Γ_F, whilst still being subcritical $\Gamma_W < \Gamma_F$. At an increased forcing frequency droplets of a certain size become unstable in their bouncing state and begin to walk. The walker then interacts with its previously generated wave fields and the interplay between the two dictates the path the droplet takes, because of its path memory. It's the walker pilot-wave dynamics that is the most similar to quantum phenomena, as the behaviour of these walkers mimics that of quantum particles. In order to consider the walking behaviour of the droplet, horizontal motion now needs to be accounted for.

The inclusion of walkers to the model developed thus far will alter the derivation of the pressure term, $\mathbf{P}_D$, seen in (2.6)-(2.9). As we aim to replace this term with the work done by the lubrication theory model (as discussed earlier in this chapter) we can implement the effect of the horizontal kick from the walkers pilot-wave simultaneously.

4.2 Numerical Improvements

The rest of this chapter will now talk about the steps we aim to take to improve the numerical simulations. The full problem that we aim to consider is very computationally heavy, with similar codes for axisymmetric problems taking a few days to run [3]. We discuss a few different routes that should be considered moving forward.

4.2.1 Integrating Factor

A way to speed up the computational efficiency of the code would be to include the method of integrating factor laid out in Milewski & Tabak [16]. This method is useful for weakly nonlinear

problems as it assumes a linear solution reducing the problem down to a single equation through a few steps. We introduce an overview of the method below.

For the system of equations in Fourier space

$$\hat{\phi}_t = -g(t)\hat{\eta} - \frac{\sigma}{\rho}k^2\hat{\eta} - 2\nu k^2\hat{\phi} - \frac{1}{\rho}\hat{P}_D \tag{4.1}$$

$$\hat{\eta}_t = k\hat{\phi} - 2\nu k^2\hat{\eta} \tag{4.2}$$

perform a change of variables

$$\hat{u} = \hat{\eta} + i\frac{k}{\omega}\hat{\phi}$$

where $\omega = \sqrt{k(g - \frac{\sigma}{\rho}k^2)}$, so that the stiff part of the equation is not only linear, but linear with constant coefficients. This reduces it down to an easily integrable equation.

$$\begin{aligned}
\hat{\phi}_t &= -\left[g(t) + \frac{\sigma}{\rho}k^2\right]\hat{\eta} - 2\nu k^2\hat{\phi} - \frac{1}{\rho}\hat{P}_D(t) \\
i\frac{k}{\omega}\hat{\phi}_t &= -i\frac{k}{\omega}\left[g + g\Gamma\cos(\omega_0 t) + \frac{\sigma}{\rho}k^2\right]\hat{\eta} - i\frac{k}{\omega}2\nu k^2\hat{\phi} - i\frac{k}{\omega\rho}\hat{P}_D(t) \\
\hat{\eta}_t + i\frac{k}{\omega}\hat{\phi}_t &= k\hat{\phi} - 2\nu k^2\hat{\eta} + -i\frac{k}{\omega}\left[g + g\Gamma\cos(\omega_0 t) + \frac{\sigma}{\rho}k^2\right]\hat{\eta} - i\frac{k}{\omega}2\nu k^2\hat{\phi} - i\frac{k}{\omega\rho}\hat{P}_D(t) \\
\hat{u}_t &= -i\frac{k}{\omega}\left[g\Gamma\cos(\omega_0 t)\hat{\eta} - i\frac{k}{\omega\rho}\hat{P}_D\right] - (2\nu k^2 + i\omega)\hat{u}
\end{aligned}$$

This can then result in the equation

$$\frac{d}{dt}\left[\hat{u}e^{(i\omega+2\nu k^2)t}\right] = -i\frac{k}{\omega}\left(g\Gamma\cos(\omega_0 t)\hat{\eta} + \frac{1}{\rho}\hat{P}_D(t)\right)e^{(i\omega+2\nu k^2)t} \tag{4.3}$$

which is the dimensional version of the one found in the Milewski paper [15] stated below.

$$\frac{d}{dt}\left[\hat{u}e^{(i\omega+2\epsilon k^2)t}\right] = -i\frac{k}{\omega}(\Gamma\cos(4\pi t)\hat{\eta} + Bo\hat{P}_D(t))e^{(i\omega+2\epsilon k^2)t}$$

This ODE (4.3) can then be solved with the usual Runge-Kutta method, however it is worth noting that in the absence of the pressure term P_D and vibrational forcing $\Gamma = 0$ then no numerical methods are needed.

4.2.2 Grid Refinement

One of the issues that arises with the current structure of the coding - and some of the numerical methods that are used to solve this problem - is the spatial grid that is being solved on.

If we consider a dimensional domain of this problem, then a 0.1 m bath with a droplet of radius 3.8×10^{-4} m would require a uniform grid with 512 nodes in each dimension to have a decent number of mesh points covering the droplet (≈ 10) rather than 256 (≈ 2), see Figure 13 for a visual guide. However there is still an entire domain that is being calculated with often not much movement occuring, especially towards the boundaries (see figure 7). A solution to this problem could be to attempt to include a non-uniform grid in the computation. Given the magnitude of the droplet radius and thus area excited by the Faraday waves is small in relation to the entire domain, a non-uniform grid with a localised concentration of points in the areas of interest would keep the number of grid points low whilst still having a high resolution simulation of the wave interface. However this sort of non-uniform grid spacing isn't compatible with the spectral method so we would have to turn to alternative numerical schemes.

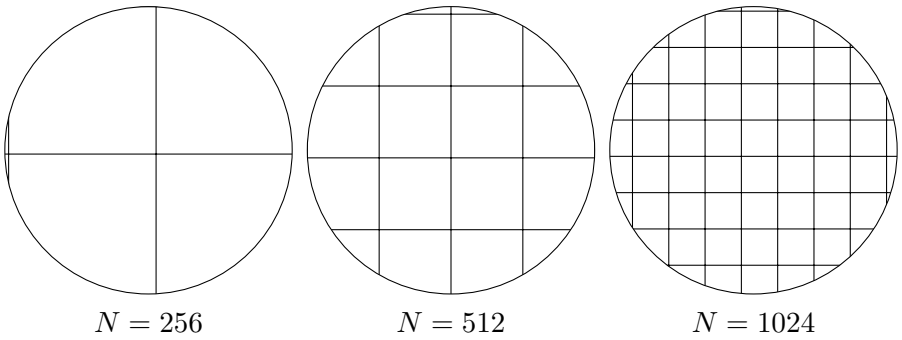

Figure 13: Visualisation of grid points of free surface affected by droplet pressure term for a square bath of length 0.1cm, and droplet radius 0.38mm

4.2.3 Alternative Numerical Scheme

The standard numerical method used for this problem by Milewski [15], [16] and Galeano [12], whose papers we followed throughout this TFR, is the pseudospectral method coupled with Runge-Kutta for the time-stepping. However it could be of interest to consider a different numerical scheme, and compare the efficiency of both. Similar to the spectral method are the finite element (FEM), finite difference (FDM) or finite volume methods (FVM). The difference between finite elements and the spectral method is the basis functions used in each. The FEM basis functions are non-zero only on small portions of the domain, rather than the global nonzero basis functions in spectral methods. As these families of methods are very similar and built upon the same foundations, it would be an interesting comparison of the numerical methods for this specific problem to compare the spectral,speudospectral and FE methods in efficiency and accuracy.

Furthermore, when considering the grid refinement spoken about earlier in this chapter, in FEM the use of non-uniform grid points is well understood and utilised in comparison to the spectral method. Thus one path of research that could be undertaken is a consideration of the different grid refinements that can be done within the different schemes.

Historically FEM has had success with elliptic and parabolic PDEs, and has somewhat lagged behind when considering hyperbolic problems such as wave propagation, or shocks travelling along characteristics. FEM and FDM often produce similar results in these cases, as such there is no universal method to consider wave problems with FEM. It is of interest then to fully consider whether this route is applicable to the problem being considered or if making improvements to the spectral method currently used is a better route.

4.3 Closing Remarks

In this report we have performed a review of the history of Faraday pilot-wave dynamics, developed a numerical code using spectral methods to model the evolution of the free surface of a Faraday-forced bath subject to a forced pressure term. We also developed a system of equations to model the pressure transfer within the air layer by treating it as a lubrication layer between a fluid bath and a hydrophobic sphere. Furthermore we discussed the different directions in which we plan on taking this project in the future, suggesting a few different mathematical routes to take, but also methods to consider and develop when working on the numerical simulation of the system of equations we produce.

References

[1] Thomas Brooke Benjamin and Fritz Joseph Ursell. The stability of the plane free surface of a liquid in vertical periodic motion. *Proceedings of the Royal Society of London. Series A. Mathematical and Physical Sciences*, 225(1163):505–515, 1954.

[2] John WM Bush. Pilot-wave hydrodynamics. *Annual Review of Fluid Mechanics*, 47:269–292, 2015.

[3] Radu Cimpeanu. personal communication.

[4] Yves Couder and Emmanuel Fort. Single-particle diffraction and interference at a macroscopic scale. *Physical review letters*, 97(15):154101, 2006.

[5] Yves Couder, Suzie Protiere, Emmanuel Fort, and Arezki Boudaoud. Walking and orbiting droplets. *Nature*, 437(7056):208–208, 2005.

[6] L. De Broglie. Ondes et mouvements. 1926.

[7] Matthew Durey and Paul A Milewski. Faraday wave–droplet dynamics: Discrete-time analysis. *Journal of Fluid Mechanics*, 821:296–329, 2017.

[8] Matthew Durey, Paul A Milewski, and John WM Bush. Dynamics, emergent statistics, and the mean-pilot-wave potential of walking droplets. *Chaos: An Interdisciplinary Journal of Nonlinear Science*, 28(9):096108, 2018.

[9] A Eddi, A Decelle, E Fort, and Y Couder. Archimedean lattices in the bound states of wave interacting particles. *EPL (Europhysics Letters)*, 87(5):56002, 2009.

[10] Antonin Eddi, Eric Sultan, Julien Moukhtar, Emmanuel Fort, Maurice Rossi, and Yves Couder. Information stored in faraday waves: the origin of a path memory. *Journal of Fluid Mechanics*, 674:433, 2011.

[11] Carlos A. Galeano-Rios, Radu Cimpeanu, Isabelle A. Bauman, Annika MacEwen, Paul A. Milewski, and Daniel M. Harris. Capillar-scale solid rebounds: experiments, modelling and simulations. submitted.

[12] Carlos A Galeano-Rios, Paul A Milewski, and J-M Vanden-Broeck. Non-wetting impact of a sphere onto a bath and its application to bouncing droplets. *Journal of Fluid Mechanics*, 826:97–127, 2017.

[13] Daniel M Harris, Julien Moukhtar, Emmanuel Fort, Yves Couder, and John WM Bush. Wavelike statistics from pilot-wave dynamics in a circular corral. *Physical Review E*, 88(1):011001, 2013.

[14] Krishna Kumar and Laurette S Tuckerman. Parametric instability of the interface between two fluids. *Journal of Fluid Mechanics*, 279:49–68, 1994.

[15] Paul A Milewski, Carlos A Galeano-Rios, André Nachbin, and John WM Bush. Faraday pilot-wave dynamics: Modelling and computation. *Journal of Fluid Mechanics*, 778:361–388, 2015.

[16] Paul A Milewski and Esteban G Tabak. A pseudospectral procedure for the solution of nonlinear wave equations with examples from free-surface flows. *SIAM journal on scientific computing*, 21(3):1102–1114, 1999.

[17] Jan Moláček and John WM Bush. Drops walking on a vibrating bath: towards a hydrodynamic pilot-wave theory. *Journal of Fluid Mechanics*, 727:612–647, 2013.

[18] Anand U Oza, Rodolfo R Rosales, and John WM Bush. A trajectory equation for walking droplets: hydrodynamic pilot-wave theory. *Journal of Fluid Mechanics*, 737:552–570, 2013.

[19] S Protière and Y Couder. Orbital motion of bouncing drops. *Physics of Fluids*, 18(9):091114, 2006.

[20] Jearl Walker. Drops of liquid can be made to float on liquid-what enables them to do so. *Scientific American*, 238(6):151, 1978.